SUBJECT-SPECIFIC HUMAN KNEE FEA MODELS FOR TRANSTIBIAL AMPUTEE VS CONTROL TIBIAL CARTILAGE PRESSURE IN GAIT, CYCLING and ELLIPTICAL TRAINING

A Thesis

presented to

the Faculty of California Polytechnic State University,

San Luis Obispo

In Partial Fulfillment

of the Requirements for the Degree

Master of Science in Mechanical Engineering

by

Ali Yazdkhasti

August 2023

COMMITTEE MEMBERSHIP

TITLE:	Subject-specific Human Knee FEA Models for Transtibial Amputees Vs Control Tibial Cartilage Pressure in Gait, Cycling and Elliptical Training
AUTHOR:	Ali Yazdkhasti
DATE SUBMITTED:	August 2023
COMMITTEE CHAIR:	Scott Hazelwood, Ph.D Professor of Biomedical Engineering
COMMITTEE MEMBER:	Stephen Klisch, Ph.D Professor of Mechanical Engineering
COMMITTEE MEMBER:	Mohammad Noori, Ph.D Professor of Mechanical Engineering

ABSTRACT

Subject-specific Human Knee FEA Models for Transtibial Amputees Vs Control Tibial Cartilage Pressure in Gait, Cycling and Elliptical Training

Ali Yazdkhasti

Millions of individuals around the globe are impacted by osteoarthritis, which is the prevailing type of arthritis. This condition arises as a result of gradual deterioration of the protective cartilage that safeguards the ends of the bones. This is especially true of transtibial amputees, who have a significantly higher incidence of osteoarthritis of the knee in their intact limb than non-amputees. Engaging in regular physical activity, managing weight effectively, and undergoing specific treatments can potentially slow down the advancement of the disease and enhance pain relief and joint function. Nevertheless, the relationship between the type of exercise and its impact on cartilage stress remains uncertain. In order to address this question, tibiofemoral finite element analysis (FEA) models were developed. The models incorporated more realistic material properties for cartilage, hexahedral elements, and non-linear springs for ligaments. To ensure their accuracy, the models were validated against experimental data obtained from cadaveric studies. The contact loads and flexion angles of two individuals with amputations and one individual without amputation, which were obtained in a previous study conducted at Cal Poly, were implemented in the FEA models for gait, cycling, and elliptical exercises. The FEA models were used to extract the maximum stress values experienced in the tibial contact areas, specifically in the medial and lateral compartments of the knee. In cycling, the normalized contact pressure on the tibial articular cartilage, relative to body weight, was generally higher for the two participants with amputations compared to the control participant, except for the medial compartment. Furthermore, when comparing different exercises, cycling resulted in the lowest contact pressure values, with elliptical and walking exercises producing similar maximum values. The findings indicated that individuals with amputations are at a greater risk of developing OA, regardless of the type of exercise performed. However, among the different exercises studied, cycling was found to exert the lowest levels of compression stress on the tibial cartilage.

Keywords: Osteoarthritis, Finite Element Analysis, human knee, transtibial amputee, gait, cycling, elliptical, articular cartilage

ACKNOWLEDGMENTS

I consider myself fortunate to have had the unwavering support and guidance of Dr. Scott Hazelwood and Dr. Stephen Klisch as my advisors during my master's thesis. I am incredibly grateful to my advisors for their exceptional support and their relentless efforts in assisting me in advancing this thesis. I cannot thank them enough for their invaluable contributions throughout this process.

Thank you to my parents, who have made countless sacrifices to ensure that I never feel lacking in any aspect of my life.

TABLE OF CONTENTS

Section Page

LIST OF TABLES

Table Page

LIST OF FIGURES

Figure Page

1. Introduction

1.1 Motivation

Osteoarthritis (OA) is a collection of conditions that lead to symptoms associated with reduced structural integrity and mechanical performance of articular cartilage (AC) in addition to related changes in the underlying bone [1]. A 2015 study of adults with and without OA estimates the direct costs of OA to be $45 billion related to health care and $1.7 billion in lost wages [2].

There is currently no cure for OA, most physicians will recommend several therapies to treat OA symptoms. These treatments are commonly physical activity therapies to activate biological signals for the health of AC. Approximately 32.5 million Americans suffered from OA in 2020, a population largely composed of adults over the age of 45 and military veterans [3]. Preventative measures that can help to mitigate the number of people suffering from this disease are of extreme interest [4], [5].

Transtibial (TT) amputees have a significantly higher incidence of OA of the tibiofemoral (TF) joint of the intact limb than non-amputees [6]. Research suggests that following injury or an amputation a compensation mechanism occurs where in the intact limb the loading becomes excessive. [7]. This abnormal loading of the TF joint may induce an accelerated degradation of AC [8-9]. The goal of this study was to investigate the pressure on the articular cartilage tissue of the intact limb in transtibial amputees and also a control group while doing common exercises including gait, stationary cycling, and elliptical training.

Finite element analysis (FEA) is the method of choice to model joint stresses and soft tissue responses due to the infeasibility of making these measurements using in vivo studies. Extensive efforts have been developed to predict in vivo cartilage behavior and address its application to clinical diagnosis and prognosis [10-14]. Earlier models considered only a group of known phenomena depending on the particular aspects of interest [15-17]. For instance, the first studies of cartilage mechanics based on the theory of linear elasticity were not able to predict the time-dependent response of the tissue. Viscoelastic monophasic models were then introduced to describe the time-dependent stress-strain relation of the tissue without explicit consideration of the interstitial fluid flow [18]. One previous study investigated the effects of different cartilage material models of finite element predictions using linear, poroelastic, and

transversely isotropic poroelastic models [19]. Although these isotropic homogenous material models are the most feasible and straightforward to implement, they may not accurately predict the behavior of a highly non-linear material like cartilage [20-25].

One of the most used theories for biological tissue is the quasilinear viscoelastic theory [26] where the biphasic and fibril-reinforced models are introduced. This model brought out success in predicting the time-dependent mechanical response of the tissue. In other studies, whole joint models have been used to investigate how altered biomechanics due to factors such as ligament reconstructive surgery and obesity impact cartilage stress [27-28]. The present study will add to the latter group, creating whole knee FEA models with advanced cartilage material models to analyze the effects of amputation status and exercise type on cartilage contact pressures (CCPs) and locations.

The primary hypothesis is that under loads from gait, tibial cartilage compartments experience the largest contact pressure magnitude over the largest area compared to cycling and elliptical training. It is also expected that differences in the magnitude and direction of the pressure applied to the intact joint lead to higher tibial contact pressure for amputees in all three different exercises compared to those of the control group [7]. Previous studies to examine this have been based on linear material models that cause some minor inconsistencies with the experimental results [30]. To address this issue, the anisotropic properties of articular cartilage tissue were taken into account in this current study when creating whole knee FEA models for both transtibial amputees and control subjects participating in gait, cycling and elliptical exercises.

1.2 Prior Work

The FEA method has found widespread application in physiological loading scenarios. FEA models offer comparable outcomes to invasive in-vivo studies. Numerous studies in literature extensively explore the modeling of various materials and components within a TF joint [31-36]. Additionally, there are other studies that propose methodologies for generating comprehensive joint models as a whole [37], [38].

This paper builds upon a series of previous studies, starting with Wangerin in [39], that collectively form a body of research conducted by the Cal Poly HMB lab. These papers focus on the

development of FEA models for the human tibiofemoral joint. Each paper in the series has played a role in the achievements of the proposed framework.

Wangerin [39] created a FEA model for the human tibiofemoral joint. This model incorporated joint contact forces obtained from motion analysis data. To construct the model, Wangerin utilized geometry data from the publicly available Open Knee repository and motion analysis data from a single participant who closely resembled the donor of the tibiofemoral joint. The primary goal of this study was to develop a comprehensive and validated FEA model of the tibiofemoral joint that could accurately predict stress and strain in the articular cartilage during walking.

The automation of the computational meshing process and FEA model generation was initiated by Lane [40]. In a groundbreaking achievement, Lane successfully constructed a robust model solely from Magnetic Resonance Images (MRIs), utilizing subject-specific loads and boundary conditions provided by the HMB lab. This model was utilized to compare cartilage contact pressure under different loading conditions during gait and stationary cycling, specifically between transtibial amputees and individuals without amputations. It is important to note, however, that this analysis was conducted using a single tibiofemoral geometry and focused on resultant loads across the knee rather than the actual contact forces exerted at the tibiofemoral joint. Furthermore, Lane initially described the mechanical properties of cartilage as an isotropic elastic material. However, these properties were unable to accurately replicate the true behavior of cartilage under mechanical loads. Nonetheless, this approach offered the advantage of lower computational costs for FEA simulations. In contrast, this current study takes a significant step forward by assigning a more realistic material model to cartilage, resulting in a better representation of its behavior. By incorporating this material model of cartilage, a better understanding of the cartilage mechanical response may be found under various loads.

Stearns [30] built upon Lane's previous research by expanding the scope and methodology. Stearns conducted a study using MRIs of three individuals (two amputees and one control) to create three tibiofemoral joint models. Instead of relying on joint reaction loads, he utilized joint contact loads for the loading conditions. Stearns then proceeded to compare the effects of three exercise types (gait, cycling, and

elliptical training) on the same subject, and assessed any disparities between the control group and the amputee group for each exercise.

Stender [41] generated a User Material subroutine in the finite element software Abaqus (Dassault Systemes, Vélizy-Villacoublay, France) that forms the foundation of this current study, focusing on cartilage. In the study, Stender formulated a polyconvex continuum-level proteoglycan Cauchy stress function, which was based on the continuum electromechanical Poisson-Boltzmann cell model for proteoglycan interactions (Appendix A). Additionally, he integrated this proteoglycan model with a unique collagen fibril model and a ground substance matrix material. The culmination of these efforts resulted in the development of a polyconvex constitutive finite element model for articular cartilage.

According to Wilson [42], the depth-dependent compressive equilibrium characteristics of articular cartilage are not caused by depth-dependent material properties, but rather by its depth-dependent composition. As a result, there is no longer a need to assume that the material properties of the various constituents themselves vary with depth. These insights are crucial for comprehending the mechanical behavior of cartilage, the mechanisms of cartilage damage, and tissue engineering research related to cartilage.

1.3 Objectives

The aim of this study is to examine variances in cartilage contact pressure among different exercise types and compare them between individuals with transtibial (TT) amputations and healthy individuals serving as controls. Gait, cycling, and elliptical training are chosen as three prevalent and easily accessible exercise forms that offer distinct loading methods: gait involves impact and weight bearing, while cycling and elliptical training involve non-impact and non-weight bearing. Analyzing discrepancies between TT amputees and controls will help identify relative risks unique to TT amputees.

By examining disparities between the control group and TT amputee subjects, it is possible to bring attention to potential heightened risks for TT amputees in developing OA in the articular cartilage. The parameters under evaluation in this study to assess the increased risk of OA are the contact pressure and contact area that the articular cartilage endures during the exercises. The level of contact pressure is directly linked to the stress experienced by the articular cartilage. It is well-established that excessive stress

on biological tissues can lead to cellular degeneration, which plays a significant role in the development of OA.

2. Methods

This section comprises a comprehensive explanation of the research approach employed to produce whole knee FEA models to examine cartilage pressure in the knee. To obtain input data for the FEA models, one healthy and two transtibial amputee participants were recruited and invited to the Cal Poly Human Motion Biomechanics (HMB) lab for motion analysis experiments. These experiments and subsequent data analysis were performed by HMB personnel separate from this thesis.

2.1 Participant Information

The exclusion requirements for the motion analysis study were fulfilled by three male participants [40]. The control participant was selected based on having comparable demographics to the amputee group. The combined demographic information of the participants is displayed in Table 2.1.

Table 2.1. Physiological data of participants

Participant ID	Status	Dominant Leg	Age	Height (cm)	Body Mass(kg)	BMI
2016Aug12-02	Control	R	22	182	79.1	24.0
2016Nov10-01	Amputee	L	32	182	74.9	22.6
2016Nov14-02	Amputee	R	31	169	83.9	29.4

2.2 Exploration of Motion Capture Techniques and Processing of Captured Data

The movement of the participants, along with their corresponding reaction forces, were recorded by means of a motion capture system combined with either ground force plates or 6-axis load cells. The recordings were carried out following the procedures described in references [43], [44]. It is worth mentioning that motion capture systems use multiple cameras and passive markers on the human body that reflect invisible infrared light emitted by the cameras, helping to estimate the person's 3D position.

The Enhanced Helen Hayes marker set was composed of 32 markers distributed across the head, shoulders, spine, chest, hips, thighs, knees, shins, ankles, and feet. The marker placement is depicted in Fig. 2.1.

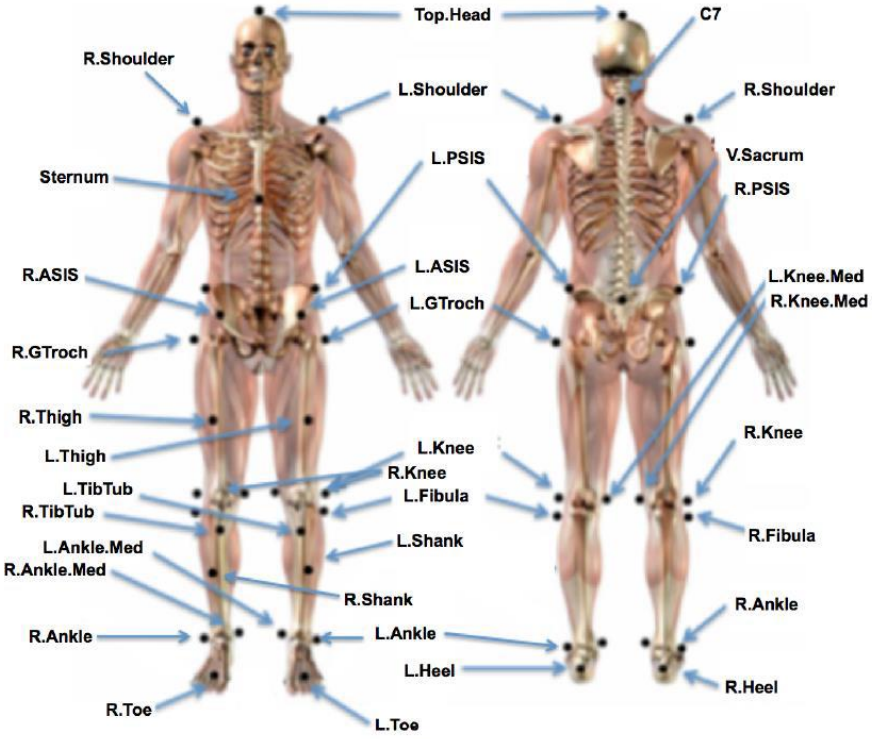

Figure 2.1. The anatomical positions of the modified Enhanced Helen Hayes markers. [45]

The study participants performed three types of exercises: gait (walking), stationary cycling, and elliptical training. To determine the joint contact boundary conditions needed for the FEA models, the motion capture data were processed using Cortex software (Motion Analysis, Rohnert Park, CA). Next, OpenSim software (Stanford University, Palo Alto, CA) [46] was utilized and followed the methodology outlined by Fernandez et al. [43] to calculate the maximum compressive loads and corresponding shear forces on the knee joint. For each exercise, the maximum compressive load in the positive direction towards the tibia was identified. The anterior-posterior (AP) shear was considered positive when directed anteriorly in the knee, and the medial-lateral (ML) shear was considered positive when directed laterally in the knee joint. These forces and corresponding knee joint angles corresponding to the position of the knee

joint center where the maximum compressive force was calculated, displayed in Table 2.2, were then used as the loading conditions in the FEA models.

Table 2.2. Participant knee joint loads and angles as calculated at the knee joint position where the maximum compressive force was determined.

Participant ID	Knee Angle [Rad]	Knee Angle [Deg]	AP Shear [N]	Compressive Force [N]	ML Shear [N]
Gait					
2016Aug12-02	0.15681	9.0	724.4	2936.4	-145.9
2016Nov10-01	0.10492	6.0	1304.1	4177.7	-120.2
2016Nov14-02	0.25039	14.3	117.2	2397.0	-102.9
Cycling					
2016Aug12-02	1.33188	76.3	174.9	558.7	48.4
2016Nov10-01	1.87134	107.2	319.5	729.9	87.2
2016Nov14-02	0.55052	31.5	-59.7	632.2	-22.8
Elliptical					
2016Aug12-02	0.64056	36.7	240.3	1658.1	-41.9
2016Nov10-01	1.16893	67.0	575.1	2034.8	-133.8
2016Nov14-02	0.50171	28.7	355.8	2960.5	-91.6

2.3 MRI Procedure

The MRI scans of the participants' knees were performed at French Hospital (San Luis Obispo, CA) on a GE Signa HDxt 1.5T scanner (GE, Chicago, IL) with the same settings for all three scans: proton density fast spin-echo, fat saturated sequence (4800 second relaxation time, 32.1 second echo, 2 averages, 90-degree flip angle) with a 1 mm slice thickness in the sagittal plane within a 512x512 matrix. The scans

were all centered on the tibiofemoral (TF) joint and included sufficient lengths of the femur and tibia to include all relevant ligament and tendon attachment sites.

2.4 MRI Post-processing

Each TF joint is comprised of eight bodies, including the femur, tibia, fibula, femoral cartilage, lateral tibial cartilage, medial tibial cartilage, medial meniscus, and lateral meniscus. These bodies are considered critical components for obtaining physiologically relevant cartilage pressure via finite element studies. To define the boundaries of the bodies in the MRI images and create a 3D surface, a segmentation process was used. Cal Poly graduate students Greg Lane, Michael Rumery, and Jon Stearns [24], [30], [40] manually performed this process for all three TF joints using ITK-SNAP (University of Pennsylvania, Philadelphia, PA). For this study, the focus was on modeling TF joints with ID numbers 2016Aug12-02, 2016Nov10-01, and 2016Nov14-02, representing a control participant and two amputee participants, respectively. Due to inadequate detail in the MRI scans, it was not possible to construct accurate representations of the ligaments; hence, they were not segmented. In these models, bones are treated as rigid bodies, while various techniques are employed to model soft tissues like ligaments. One widely used approach is to represent ligaments using a finite number of spring-like elements to represent their force contribution on the bones. However, this approach may suffer from inaccuracies owing to the limited number of fibers and their placement, even though it is an efficient and easily implementable method. Figure 2.2 displays the MRI sequences, whereas Figure 2.3 presents a sample of the 3D surfaces of the TF joint.

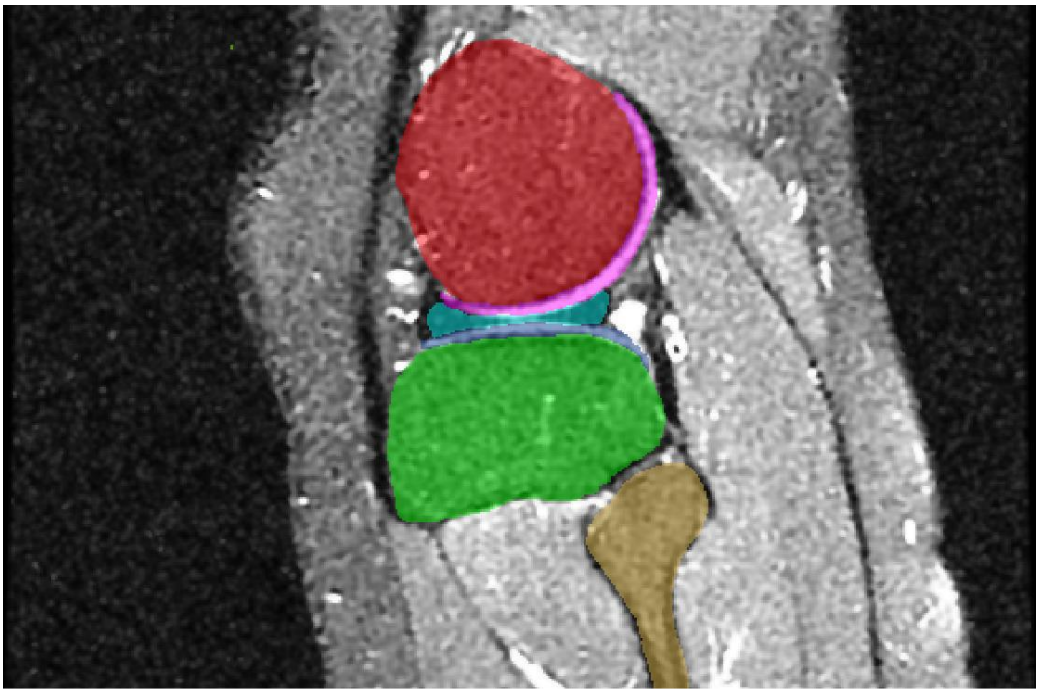

Figure 2.2. Fully segmented MRI sequence image of 2016Nov05-01R. Sagittal plane view. Femur (red), femoral cartilage (pink), lateral meniscus (teal), lateral tibial cartilage (blue), tibia (green) and fibula (tan)[39]

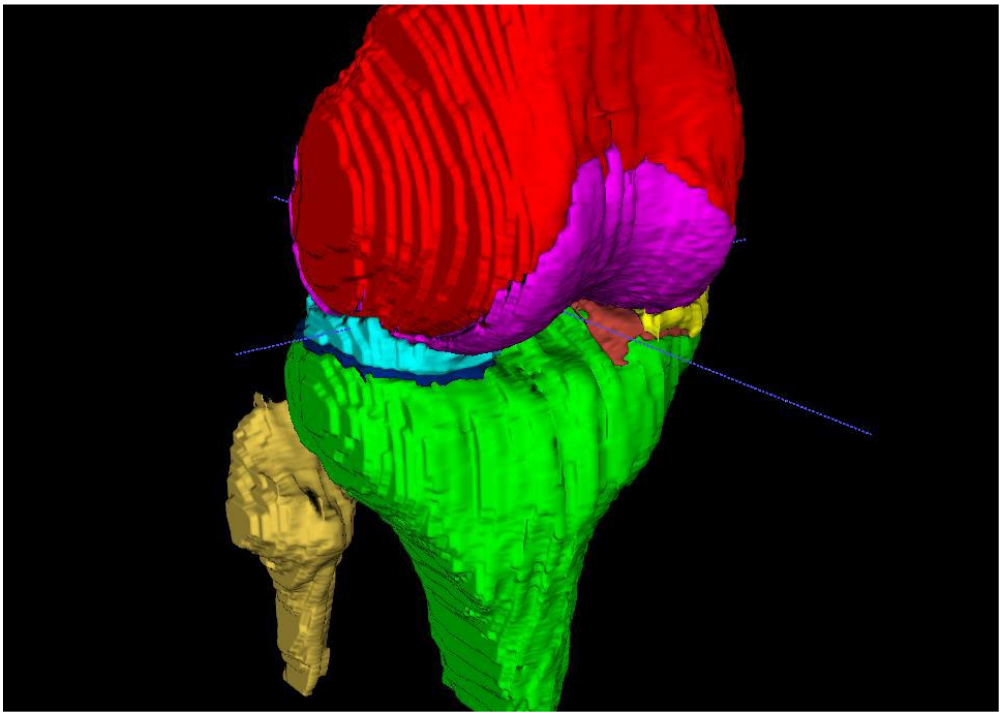

Figure 2.3. 3D surfaces of the bodies in the TF joint using ITK-SNAP [39]

2.5 Smoothing

The segmentation method used to export the 3D surfaces resulted in distorted shapes, making them unsuitable for finite element modeling. One reason for this is that the mesh must be dense enough to accurately capture the features of the structure, such as the sharp edges of the staircase artifacts that cause element distortion. However, excessively dense meshes can make FEA simulations computationally expensive, making it impractical for analysis purposes.

The work for the current thesis began by using the previously segmented surfaces of the TF joints. Here, an approach was employed whereby the surface meshes were transformed into 3D solid parts using Geomagic Design X (3D SYSTEMS, Santa Clarita, CA, USA). One common technique used by Geomagic software to smooth surfaces is called filtering. This involves applying a mathematical filter to the elevation values of the surface, which averages out small-scale irregularities while preserving larger-scale features. Another technique used in Geomagic software for surface smoothing is interpolation. This involves estimating the elevation values of a surface at unsampled points based on the values at neighboring points. Interpolation can be used to fill in gaps or missing data in a surface, as well as to smooth out irregularities by fitting a smooth function to the data.

Although smoothing has been shown to effectively reduce surface irregularities, it is imperative to acknowledge that it can also lead to a decrease in the size of the bodies. Such reduction could potentially cause the bodies to lose their contact during assembly. To counter this issue, a scaling-up approach was employed in Geomagic after the smoothing process to guarantee that the bodies remained in contact. The appropriate scaling factor was determined by analyzing the volume of material that was removed before and after the smoothing process. The scaling factor ranged between 2.0% and 2.8%, and was implemented to ensure that the desired level of contact between the bodies was achieved during assembly. The smoothing process sequence for the femoral cartilage of participant 2016Nov10-01 can be observed in Figures 2.4 to 2.6.

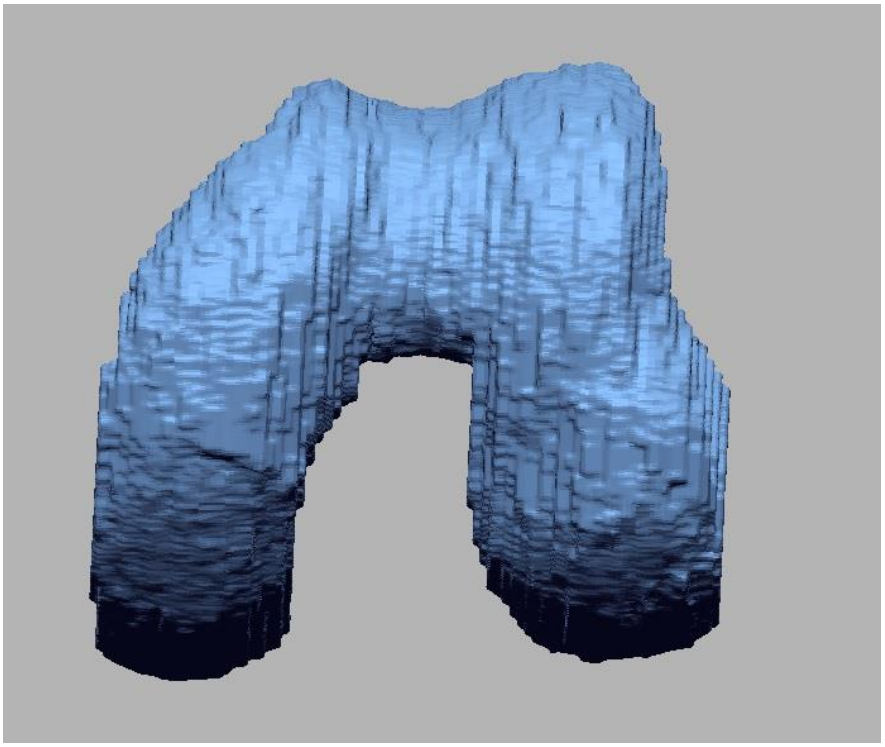

Figure 2.4. The segmented femoral cartilage imported into Geomagic.

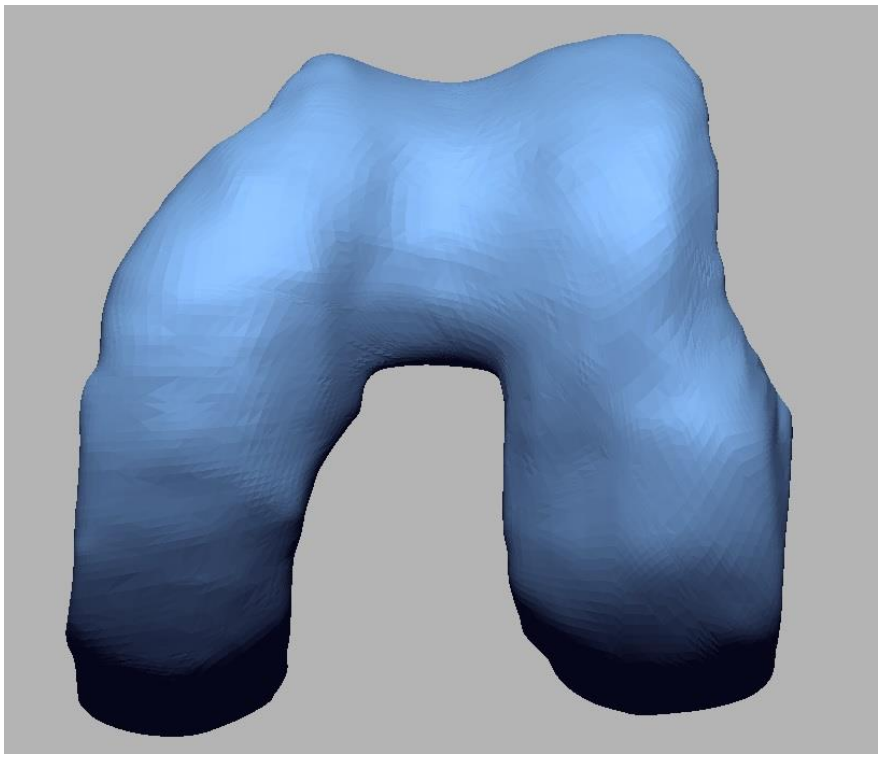

Figure 2.5. The smoothed femoral cartilage using Geomagic.

Figure 2.6. The trimmed and scaled femoral cartilage within Solidworks.

2.6 Creating the Computational Mesh

This study focused on the behavior of soft tissues, therefore bones such as the femur, tibia, and fibula were treated as discrete rigid bodies to reduce the computational cost of the simulation. It was also necessary to convert these solid bodies into shell surfaces. This is because shell elements have a lower degree of freedom than solid elements, and therefore require less computational resources during the analysis. In contrast, all other five soft tissues were considered computational continuum solid bodies.

Previous studies typically relied on secondary software, such as GMSH and TetGen, to discretize the different parts [30], [47]. The rigid surfaces were usually meshed using GMSH (GPL, Liège, Belgium) [48], while the continuum bodies were meshed using TetGen (WIAS, Berlin, Germany) [49], [50] through the Matlab extension GIBBON (MathWorks, Natick, MA). However, this approach can lead to data transfer issues, inconsistency in the mesh quality, and data conversion errors. One common error that may happen is the "ErrElemMissingSection" error [51], which indicates that the elements in the model have not

been properly assigned a section. This error typically occurs when attempting to run a simulation in Abaqus, and it can prevent the model from being analyzed correctly.

The novelty of the current study in this thesis lies in discretization of both computational and noncomputational bodies within the Abaqus environment. By meshing parts inside Abaqus, it could be ensured that the same meshing parameters and techniques were used consistently throughout the analysis. This could improve the repeatability of the analysis results and reduce the potential for errors or inconsistencies in the analysis. Also, the workflow could be streamlined and the time and effort required to prepare the model for analysis could be reduced. This resulted in faster turnaround times for simulations and reduced the overall cost of the analysis.

Abaqus FEA offers several options for defining elements that can be selected according to the requirements of the simulation. To improve the accuracy and effectiveness of the model, hexahedral elements were used instead of the tetrahedral elements used in previous studies [30], [47]. This development was made possible by the ability to mesh the parts within the Abaqus environment. Hexahedral elements are often preferred over tetrahedral elements for modeling anisotropic materials due to their higher aspect ratio. This aspect ratio enables them to more accurately represent the model's shape while maintaining a lower element count, resulting in faster computational times. Hexahedral elements also exhibit better geometric symmetry, leading to a more uniform distribution of stress and strain within the element, thereby reducing numerical errors [51], [52], [53].

2.7 Material Properties and Abaqus Assembly Module

This model consists of five soft-tissue components (femoral cartilage, medial meniscus, lateral meniscus, medial tibial cartilage, lateral tibial cartilage), three bones (femur, tibia, fibula), and four spring elements that represent the major ligaments of the joint (ACL, PCL, MCL, LCL). Each component must be associated with a specific material model within Abaqus FEA as are described in the following Table 2.3.

Table 2.3. Material models for all four different components

Component	Material model
Cartilage	Non-linear anisotropic
Meniscus	Linear-elastic isotropic
Ligaments	Non-linear axial spring
Bones	Rigid

The cornerstone of this work was modeling articular cartilage as an anisotropic material. The articular cartilage comprises a multicomponent matrix that surrounds a limited number of cells called chondrocytes. In terms of its mechanical properties, the articular cartilage is a combination of materials that exhibit significantly different characteristics. The tissue's weight is primarily composed of water, accounting for around 70 to 85% of the total cartilage weight. Most of the remaining tissue is made up of collagen and proteoglycans. Proteoglycans are composed of a protein core that forms a bottlebrush-like structure which include glycosaminoglycans (GAGs) such as chondroitin sulfate and keratan sulfate. Proteoglycans have the ability to bind or aggregate with hyaluronic acid to create a large macromolecule.

Proteoglycans constitute around 30% of the dry weight of articular cartilage, and their concentration, along with the water content, differs at various depths within the tissue. The concentration of proteoglycans is relatively low, and the water content is highest, near the articular surface. Conversely, in the deeper regions of the cartilage, near subchondral bone, the proteoglycan concentration is the highest, and the water content is at its lowest [54], [55], [56]. Collagen, which is a fibrous protein, comprises the remaining portion of the solid matrix. While other types of collagen are also present in minor quantities [57], type II collagen is the primary collagen found in articular cartilage. The arrangement of collagen fibers within the tissue differs at various depths.

Due to the complex behavior of cartilage material, the built-in material models provided in Abaqus are not sufficient to accurately represent it. To overcome this, an Abaqus user material subroutine (UMAT) was employed to define a custom mechanical constitutive behavior for the material (Appendix B).

The UMAT used was developed by Stender [41]. It includes glycosaminoglycan and matrix descriptions, as well as an elastic constitutive model for collagen. To ensure that the UMAT accurately

reflects the viscoelastic model being applied to the collagen fibers, it was updated by Griebel [34]. In this model, the viscoelastic properties of the collagen fibers were represented using a two-term Prony series expansion within the quasi-linear viscoelastic model. This model includes a continuous distribution of collagen (COL) fibers, alongside glycosaminoglycans (GAG) and matrix (MAT). The distribution of COL fibers was characterized using a normalized Gaussian distribution function. To use the UMAT subroutine in Abaqus, four parameters must be provided by the user as inputs. These parameters are defined by the user and are specific to the material being modeled.

The first parameter is collagen fiber modulus. Yang [58] reported that the modulus of collagen fibers ranged from 2.8 to 3.0 GPa. Collagen volume fraction is another variable that varies within the cartilage thickness. Alizadeh et al. [59] observed that the collagen volume fraction in cartilage decreases slightly from the superficial layer to the deeper layer, ranging from 0.197 to 0.195.

GAG density is the third parameter and is defined as a percentage of final weight. Rogers et al. [60] collected cartilage samples from 13 individuals who were having an above-knee amputation. The samples were then digested using the papain enzyme and their biochemical composition was analyzed using spectrophotometric and fluorometric assays to measure GAG and DNA levels, respectively. They found that the GAG density in the cartilage is approximately 5.2%.

The ground matrix shear modulus is the last parameter. Peters et al. [61] found that the overall cartilage shear modulus varied between 11.4 and 15 MPa.

The C3D8 elements in Abaqus possess the capacity to undergo significant deformations and rotations, which render them highly suitable for accurately modeling complex anisotropic material behavior. While C3D8R elements may offer significant computational cost savings, it is important to note that they are not compatible with UMAT due to their reduced integration algorithms. Thus, C3D8 elements were employed for all three cartilage structures in the model.

In finite element simulations of the tibiofemoral joint, linear-elastic isotropic material models are frequently employed to characterize the mechanical behavior of meniscus. In accordance with this approach, a linear material model was utilized to define the constitutive properties of these tissues in this simulation, as detailed in references [23], [40], and [53].

In Abaqus, a material is considered incompressible if its Poisson's ratio is 0.5. A Poisson's ratio for the meniscus of 0.49 in Abaqus is therefore considered to be a nearly incompressible material. To address this issue, C3D8H, the hybrid variant of 8-node linear brick elements were used. These elements combine displacement-based and pressure-based formulations to model the behavior of incompressible materials. A summary of all the material models used in the knee model is found in Table 2.4.

Table 2.4. Material Properties of Cartilage and Menisci [58-61]

Component	Material Properties	
Cartilage	Collagen fiber modulus	2.8 to 3.0 GPa
	Collagen volume fraction	0.195 to 0.197
	GAG density	5.2%
	Ground matrix shear modulus	11.14 to 15 MPa
Menisci	Poisson's ratio	0.49
	Modulus of Elasticity	59 MPa

These material properties for the articular cartilage were obtained through testing of various samples, resulting in a wide range of values. Therefore, there is no single specific value applicable to all cartilage structures across different age or gender categories. Instead, a range of values is provided to account for the inherent variability observed in different cartilage samples. To determine the appropriate value for use in the FE model, three material properties were held constant, while various values within the specified range for one property were input into the FE model for participant 2016Aug12-02. It is worth noting that apart from the ground matrix shear modulus, the observed differences in contact pressure values were negligible, amounting to less than one percent. It was found that a collagen fiber modulus of 3 GPa, a collagen volume fraction of 0.197, and a ground matrix shear modulus of 15 MPa yielded results in the FE model that closely matched the experimental data used for validation (see section 2.12). Therefore, these values were chosen.

The bones were considered rigid and were composed of R3D3 elements. These types of elements do not require material properties. As a result of the element definition, the body defined by its surface becomes computationally rigid and exhibits infinite stiffness.

CONN3D2 elements, which are specialized elements in Abaqus FEA used to simulate various mechanical connections, were employed to create the ligaments within the model. These elements acted as axial springs, with force applied along the line of action defined by the connected nodes and based on their relative displacement. To create a CONN3D2 element, several steps are involved. First, you need to select two node locations that will connect the bones together. Then, you must specify the degrees of freedom in which the connected nodes will be constrained. Finally, you need to define how the constrained degrees of freedom will affect the connected nodes during relative motion by specifying the behavior of the nonlinear spring. The approach and logic used in [1] and [10] were applied in defining this material, and its properties were computed directly from [62]. Non-linear behavior of all four ligaments was characterized by defining the relationship between force (F) and displacement (UR), which is presented in Table 2.5.

Table 2.5. Connector behavior variables for the ligaments

ACL		PCL		LCL		MCL	
F(N)	UR (mm)	F(N)	UR (mm)	F(N)	UR (mm)	F(N)	UR (mm)
0	-100	0	-100	0	-100	0	-100
5	0	5	0	5	0	5	0
1493	100	1477	100	1048	100	1468	100

The model measures the distance between nodes in millimeters and defines force in newtons. Non-linear spring behavior is incorporated, allowing for pre-tension in the ligaments, but it does not allow for resistance against compressive forces. Notably, the nonlinearity of the spring behavior was accounted for by activating the nonlinear elasticity option within Abaqus. This was accomplished by providing the forces and their corresponding displacements as input values.

2.8 Contact Interaction

The main challenge encountered while creating an FE model of the knee was the intricacy involved in the interaction between the articular surfaces. In this study, the FE models incorporated six contact interactions located in the TF joint. It is worth noting that in Abaqus, parent and child surfaces are used in contact analysis to define the interacting surfaces between two different parts or sections of a model. The parent surface is the surface that is used to calculate the contact forces and displacements, while

the child surface is the surface that is affected by these contact forces and moves in response to the parent surface. For this study, the medial and lateral tibial cartilage were designated as the parent surfaces, as these were the two primary surfaces under investigation. Table 2.6 below lists the contact pairs.

Table 2.6. List of Cartilage and Meniscus contact surfaces

Cartilage to Cartilage Contact	
Lateral femoral cartilage (Child)	lateral tibial cartilage (Parent)
Medial femoral cartilage (Child)	medial tibial cartilage (Parent)
Cartilage to Meniscus Contact	
Lateral femoral cartilage (Child)	lateral meniscus (Parent)
Lateral tibial cartilage (Parent)	lateral meniscus (Child)
Medial femoral cartilage (Child)	medial meniscus (Parent)
Medial tibial cartilage (Parent)	medial meniscus (Child)

In order to accurately represent the low-friction nature of cartilage, the contact model utilized a frictionless tangential behavior to surface and a "hard" contact normal to the surface, as outlined in sources [53], [63]. Additionally, two tie constraints were defined to approximate the physiological behavior of cartilage connected to bone through subchondral tissue. The lateral meniscus and medial meniscus are attached to the tibia by the coronary ligament, the anterior meniscotibial ligament, and the posterior meniscotibial ligament. The coronary ligament is a broad band of fibers that connects the peripheral edge of the meniscus to the tibia. The anterior and posterior meniscotibial ligaments are smaller bands of fibers that attach the anterior and posterior horns of the medial meniscus to the tibia, respectively [64]. In this model, two tie constraints were used to attach a negligible portion of the menisci to the tibia cartilage for the purpose of simplification. Although this method did not exactly simulate the attachment of the menisci to the tibia, it was utilized in the FE models to better approximate the actual tissue behavior without making the model computationally expensive.

While Abaqus does permit some degree of overlap between tied and contact surfaces, a comprehensive analysis of all three assemblies in Solidworks was conducted to detect any interferences between the components. Following this step, any penetrations from the child surfaces were removed to

create an assembly without any overlaps, which was then imported into the Abaqus environment for further analysis. This approach ensured that the model was free of any interferences that could affect convergence. Table 2.7 lists the tie constraints applied to the surfaces.

Table 2.7. Tie constraints between the surfaces

Bone to Cartilage Tie Constraints	
Femoral Cartilage	Femur
Medial Tibia Cartilage	Tibial Plateau
Lateral Tibia Cartilage	Tibial Plateau
Meniscus to Cartilage Tie Constraints	
Medial Tibia Cartilage	Medial Meniscus
Lateral Tibia Cartilage	Lateral Meniscus

2.9 Reference Point of Loading and Boundary Conditions

A reference point was required to implement loading and boundary conditions for the knee joint center and the flexion-extension axis. The midpoint of the femoral epicondyles was chosen as the reference point for the knee joint center to apply knee contact loads, while the nodes at the epicondyles of the femur were identified to determine the flexion-extension axis - the axis around which the femur rotates. An MRI scan was used to locate the extreme medial and lateral aspects of the femur, and in Abaqus, a reference coordinate system was established with the medial epicondyle as the center, and the lateral epicondyle assigned to the positive x-axis. To align with the motion analysis experimental coordinate system, a point directly below the medial epicondyle was used to define the x-y plane, resulting in a coordinate system that aligned with the experimental coordinate system. To determine the knee joint center in Abaqus, a reference point was established after taking the average coordinates of the epicondyles [40]. Figure 2.7 shows the knee joint center assigned to 2016Nov10-01.

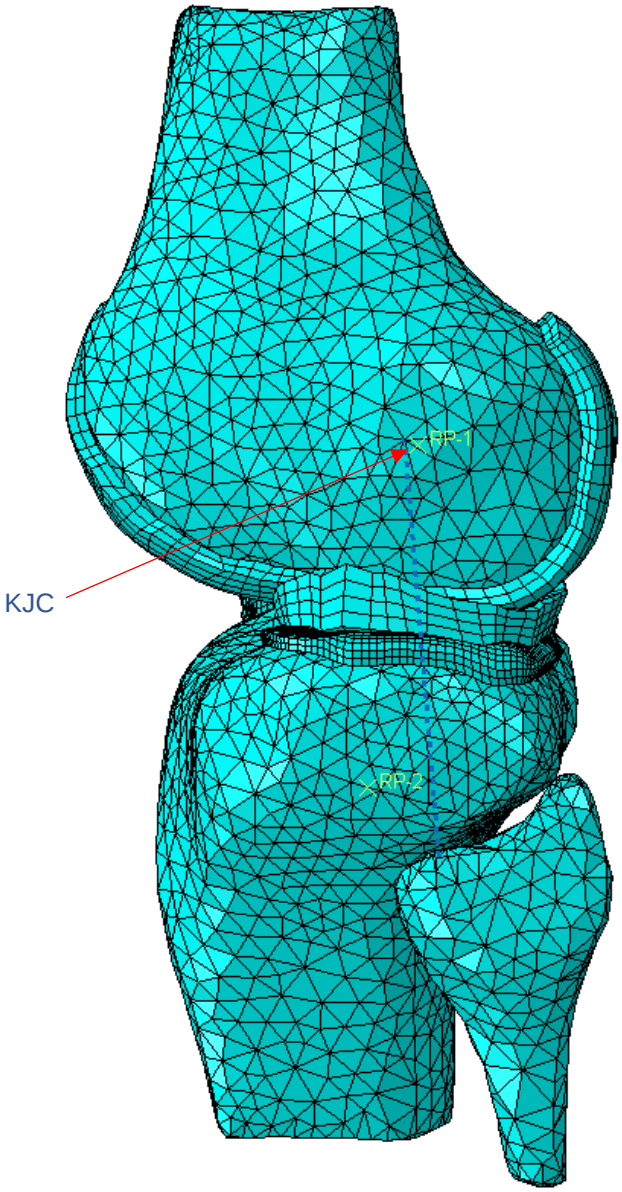

Figure 2.7. The entire knee joint assembly with its knee joint center (KJC).

2.10 Abaqus Simulation Extracting Results

In Abaqus, two output variables that can provide indications of cartilage damage are CPRESS and CAREA. CPRESS represents the magnitude of the net contact normal force per unit area, while CAREA refers to the contact area [65], [66]. Since contact stress is the primary factor responsible for cartilage degradation, the significance of contact area as an output variable was deemed to be lower.

To obtain the reported stress in Abaqus, the maximum value of CPRESS was averaged over the node of maximal contact compression stress and the 8 surrounding nodes in the four neighboring elements. This averaging technique mitigated the impact of stress concentrations and provided a more accurate representation of the cartilage stress. The method of measurement used here relies on data obtained from Seitz's experiments described in [67], which involved the use of a digital pressure sensor placed between the tibial and femoral cartilages to capture contact pressure with a spatial resolution of 1.4 mm^2. Figure 2.8 illustrates the positioning of the 9 nodes.

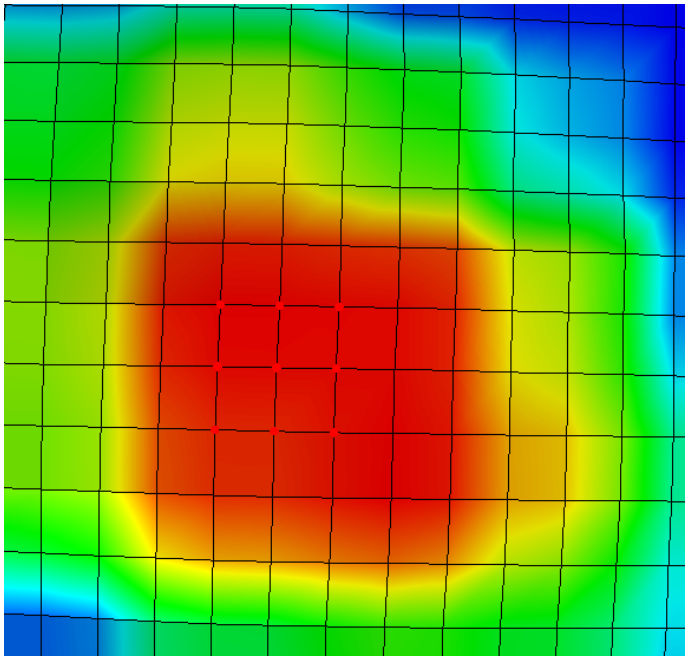

Figure 2.8. Location of the nodes utilized for contact pressure averaging.

2.11 Abaqus Step and Control Design

In Abaqus Standard, models are usually solved through a sequence of steps to account for the evolving behavior of the system being studied. When a model undergoes substantial motion or deformation, it implies significant changes in its shape or position during the simulation. These changes can result from external loads, material behavior, or other factors. To accurately capture such changes, the

model is segmented into multiple steps, with each step representing a particular loading and boundary condition in the simulation.

In the current study, the model was divided into four distinct steps: Up, Rotation, Down, and Contact. The femur reference point was the recipient of all force and displacements, which were then transmitted to the entire femur as a rigid body. The first step of the simulation involved allowing the model to reach equilibrium without applying any loads or rotations. The femur was translated 2mm up to have some translations and rotations free while tibia was fixed along all six degrees of freedom. In the second step, the femur was instructed to rotate solely around the flexion-extension axis until it reached the angle corresponding to the point of maximum compressive force during the exercise being examined. During this rotation, all other degrees of freedom were constrained. Like the first step, tibia was completely fixed.

The purpose of the third step was to correct the 2 mm transition that occurred in the first step. To achieve this, a slight force was exerted on the femur to displace it downward until it made contact with the tibial plateau. During this process, the flexion-extension angle remained constant, an applied force was exerted in the axial direction along the femur longitudinal axis, and all other degrees of freedom were constrained. In the last step, the flexion-extension angle of the femur was kept fixed while allowing the other rotational degrees of freedom to remain unrestricted. During this step, the joint contact forces were applied to the femur's three translational degrees of freedom based on the motion analysis experiment results (see Table 2.2).

UMATs typically represent nonlinear material behaviors, which can make the solution highly sensitive to changes in material properties, loading conditions, and boundary conditions. This can lead to convergence problems, as the solution may oscillate or diverge due to numerical instability, especially when the model includes large deformations, strains, or rotations. The nonlinearity of the model may also be affected by other factors such as contact sets, tie constraints, nonlinear springs, large deformations, and distorted elements.

In situations where instability affects the overall load-displacement response and leads to negative stiffness, the issue can typically be treated as a buckling or collapse problem. However, in the current model, the instability was localized to a specific area, and the strain energy was only transferred to nearby

parts, making it impossible to solve using global solution methods. Therefore, an artificial damping technique was necessary to resolve the problem. Fortunately, Abaqus/Standard provides a feature that can automatically stabilize such unstable problems by adding damping to the model in proportion to its volume. For this model, a damping factor of 2.0×10^{-4} was chosen as the default value [51].

While damping was critical for the convergence of this model, the effects of viscous forces should be monitored to ensure that they haven't affected the results. Abaqus recommends comparing the internal energy of the entire model to the static dissipation energy of the entire model. The ratio of static dissipation energy to internal energy should be less than 10% to verify the physically accurate behavior of the simulation. This procedure was implemented for all models in this study to ensure the accuracy of the results.

A common error encountered when dealing with nonlinear models is the "Too many attempts made for this increment" error which indicates the analysis diverged in its attempt to find a solution. To resolve this error, discontinuous analysis was enabled by setting the number of equilibrium iterations, I_0=8 (default I_0=4), and the number of consecutive equilibrium iterations, I_R=10 (default I_R=8). These settings could prevent early cutbacks of the time increment. Additionally, to allow for greater flexibility in the analysis, the maximum number of cutbacks permitted for an increment (I_A) was increased from its default value of 5 to 20 [51].

2.12 Convergence and Validation Study

Like any other numerical software package Abaqus uses discrete points to solve problems. Each point, or node, adds degrees of freedom (DOF) to the system, increasing its ability to capture structural behavior. However, each DOF also adds complexity and increases solve time. To ensure accurate results, it is important to demonstrate that the solution converges and is not dependent on the size of the mesh.

In this study, a mesh convergence study was performed by refining the three target cartilage regions under investigation. The menisci were excluded from the convergence study as they were not within the intended scope of this model. For each cartilage body of participant 2016Aug12-02, five meshes were created with an increasing number of elements in each iteration. The maximum CPRESS was the response of interest. To ensure accuracy, the locations of specific elements where the maximum CPRESS

was reported were adjusted so the area CPRESS examined was similar for all five mesh refinements. One advantage of using the meshing feature in Abaqus was that the convergence study was completed much faster than in previous studies where a secondary software was used to mesh parts. This resulted in significant effort being saved in preparing the model for analysis after each mesh refinement. The number of degrees of freedom for each cartilage body are detailed in Table 2.8 below.

Table 2.8. Number of degrees of freedom in each cartilage body for the mesh convergence analysis.

	Mesh 1	Mesh 2	Mesh 3	Mesh 4	Mesh 5
Femoral Cartilage	6212	9748	17012	23274	27516
Lateral Tibial Cartilage	1092	2001	3138	6003	7082
Medial Tibial Cartilage	1185	2271	3204	6339	7428

A validation study is a way to check how well a model can simulate a real-life scenario by comparing its results to the actual behavior of the scenario. Because models are approximated using numerical algorithms, they can't perfectly reflect the original system. The goal is to make sure the simulation is accurate enough for its intended use. This is done by checking the accuracy of the material being modeled against known experimental data. For this study, model results from participant 2016Aug12-02 were compared to the experimental data acquired by Seitz et. al. [67].

To replicate the experimental configuration employed by Seitz et al., two uniaxial compressive forces of 500N and 1000N were applied to the knee joint center (KJC), that is, the reference point designated on the femur. The boundary conditions were established such that the tibia was fully constrained while the femur was restricted from rotating with respect to the flexion-extension axis. As described, in this configuration, a force sensor resistor with a surface area of 140 mm^2 was implanted between the menisci and tibial cartilage for the purpose of detecting the pressure exerted on the cartilage surface (CPRESS).

3. Results

3.1 Mesh convergence

The results of the mesh convergence analysis are presented in Figures 3.1, 3.2, and 3.3. The vertical line in the graphs below indicates the point where further mesh refinement does not significantly alter the solution (0.05% to 0.95% difference from mesh 4 to mesh 5 for each cartilage structure).

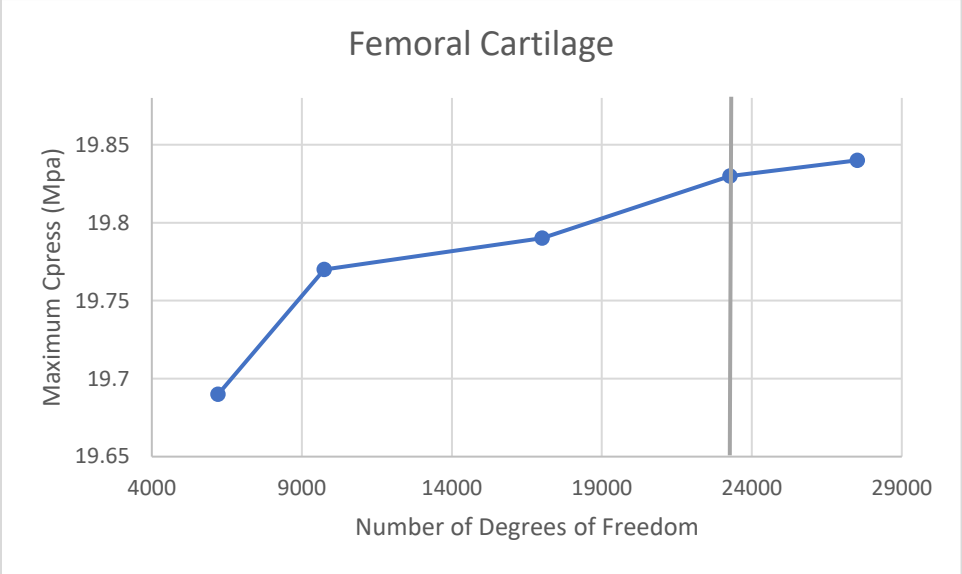

Figure 3.1. Maximum CPRESS on femoral cartilage reported at different mesh sizes.

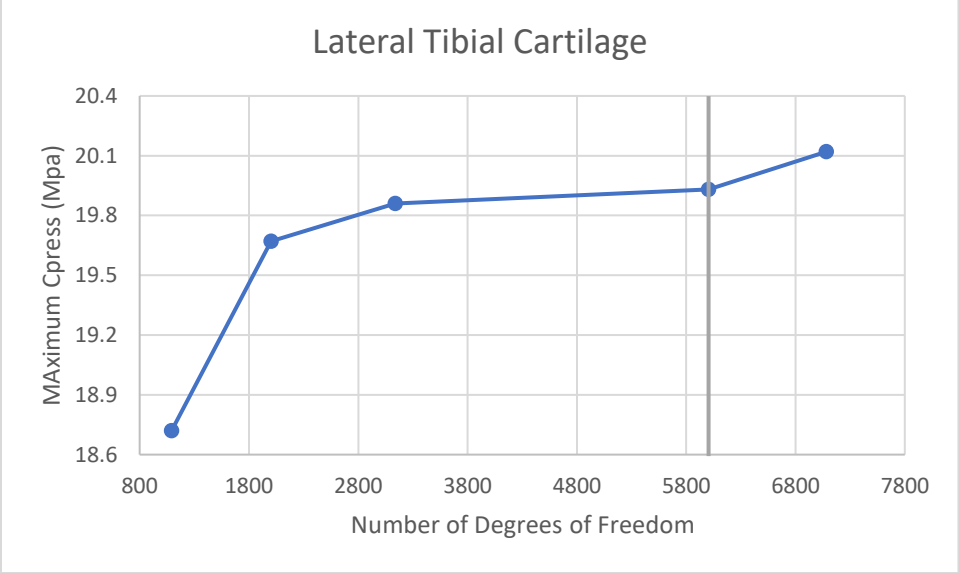

Figure 3.2. Maximum CPRESS on lateral tibial cartilage reported at different mesh sizes.

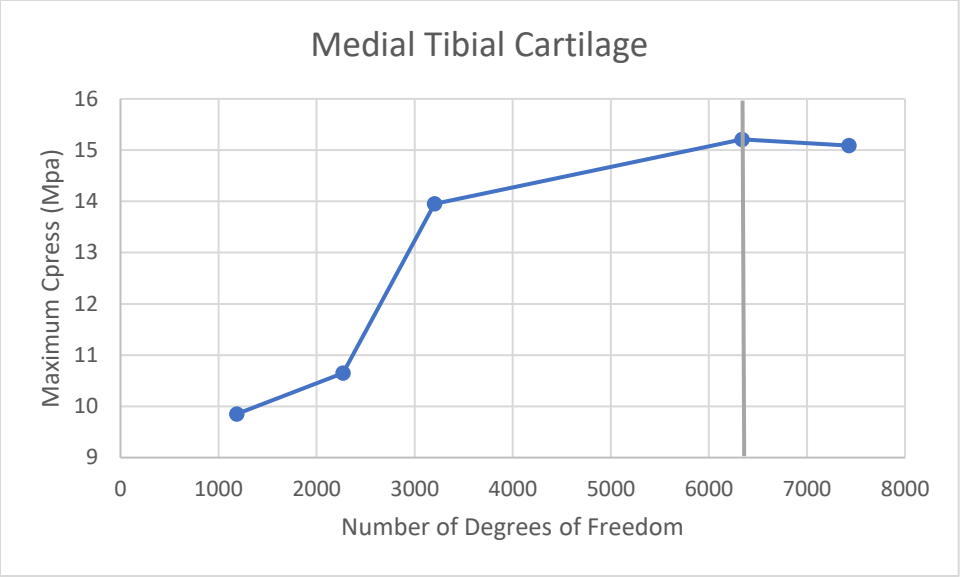

Figure 3.3. Maximum CPRESS on medial tibial cartilage reported at different mesh sizes.

3.2 Validation Studies

Table 3.1 displays the results obtained from the validation studies conducted with both 500 N and 1000 N compressive loads, with results from each compartment falling within one standard deviation of the experimental mean (less than 13.8% difference between the FEA results and the experimental mean values).

Table 3.1. Validation study cartilage pressure results for 500 N and 1000 N compressive loads

MPa	Seitz et al.- 500 N			FEA
	Mean-SD	Mean	Mean+SD	
Medial Tibial	1.18	1.78	2.38	1.61
Lateral Tibial	0.97	1.79	2.61	1.85

MPa	Seitz et al.- 1000 N			FEA
	Mean-SD	Mean	Mean+SD	
Medial Tibial	1.95	2.82	3.69	3.13
Lateral Tibial	1.72	3.04	4.36	3.46

3.3 Material Parameter Study

Experimental data from Seitz et al. [67] were utilized to determine the specific material property value within a given range that would align with one standard deviation from the experimental mean contact pressure value. Table 3.2 presents the findings of a material study that centered on a particular variable: the shear modulus of the ground matrix. The results indicated that 15 MPa was the suitable value that provided a contact pressure within one standard deviation from the mean value for both compartments of the joint.

Table 3.2. Material Parameter Study

MPa	Seitz et al.- 500 N			Ground Matrix Shear Modulus Variable used in FEA			
	Mean-SD	Mean	Mean+SD	12 MPa	13 MPA	14 MPa	15MPa
Medial Tibial	1.18	1.78	2.38	0.91	1.06	1.13	1.61
Lateral Tibial	0.97	1.79	2.61	0.98	1.19	1.41	1.85

3.4 FE Simulations

The contour plots for each model simulated are shown in Figures 3.4 through 3.12. The actual and normalized (by body weight) contact pressure (CPRESS) [MPa] results are listed in Tables 3.3, 3.4, and 3.5.

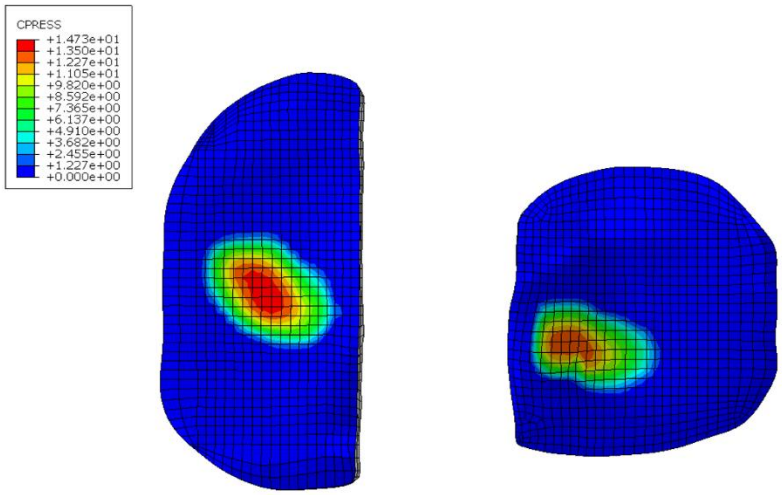

Figure 3.4. Contour plot reporting CPRESS for medial (left) and lateral (right) tibia cartilage pressure for gait results obtained for participant 2016Aug12 (control)

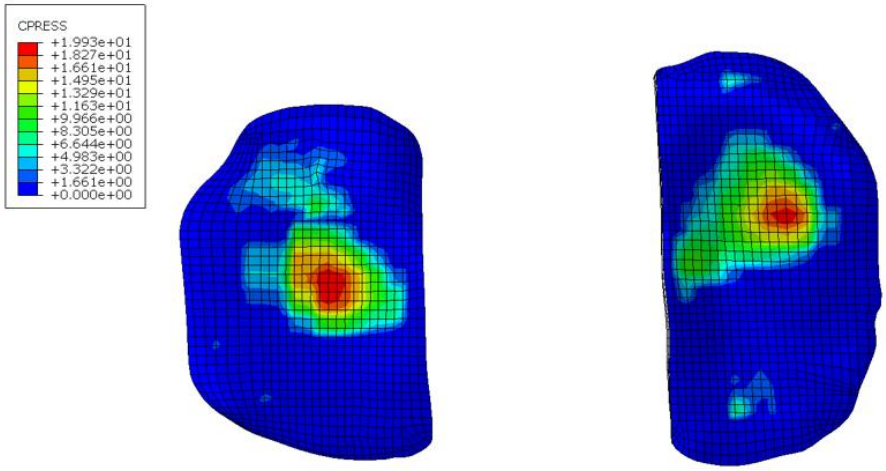

Figure 3.5. Contour plot reporting CPRESS for lateral (left) and medial (right) tibia cartilage pressure for gait results obtained for participant 2016Nov10 (amputee)

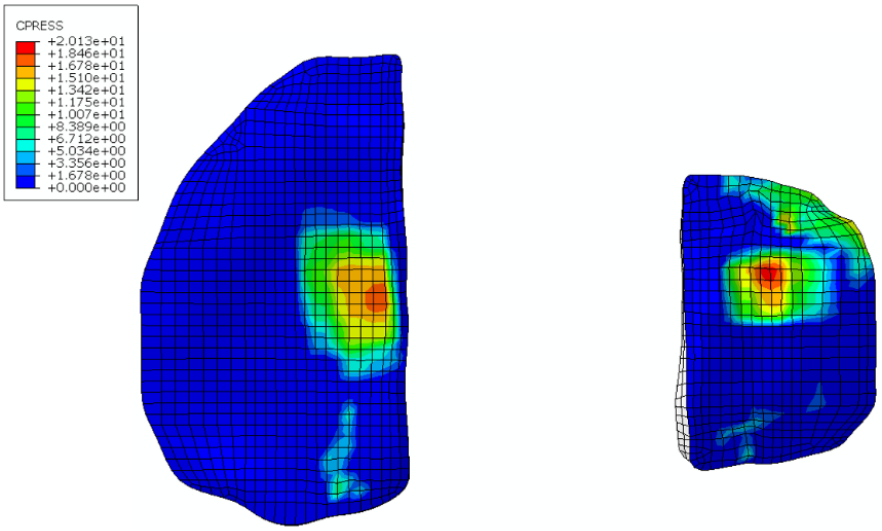

Figure 3.6. Contour plot reporting CPRESS for medial (left) and lateral (right) tibia cartilage pressure for gait results obtained for participant 2016Nov14 (amputee)

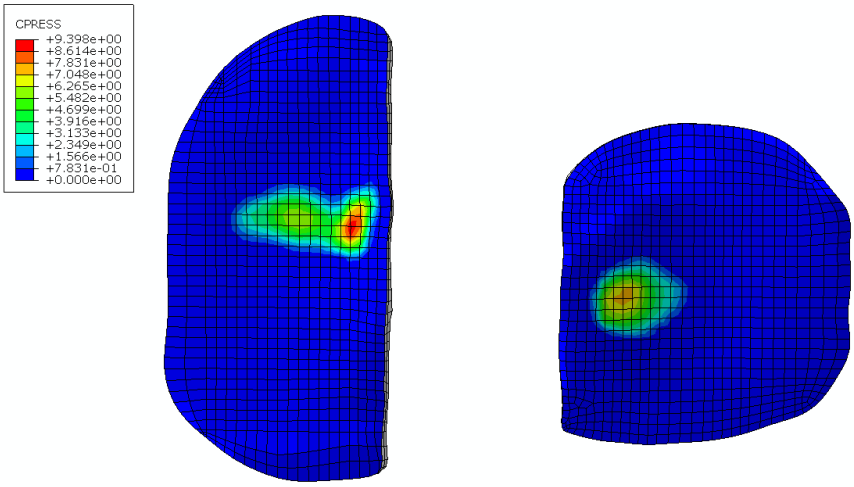

Figure 3.7. Contour plot reporting CPRESS for medial (left) and lateral (right) tibia cartilage pressure for cycling results obtained for participant 2016Aug12 (control)

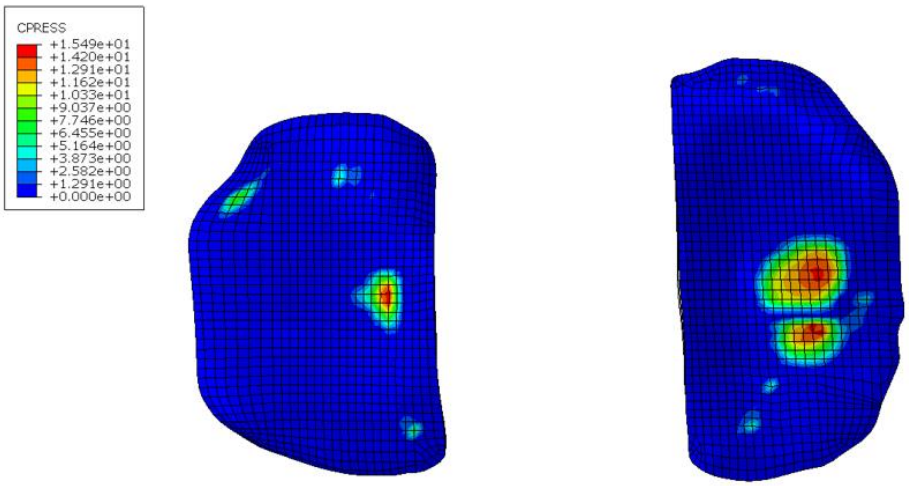

Figure 3.8. Contour plot reporting CPRESS for lateral (left) and medial (right) tibia cartilage pressure for cycling results obtained for participant 2016Nov10 (amputee)

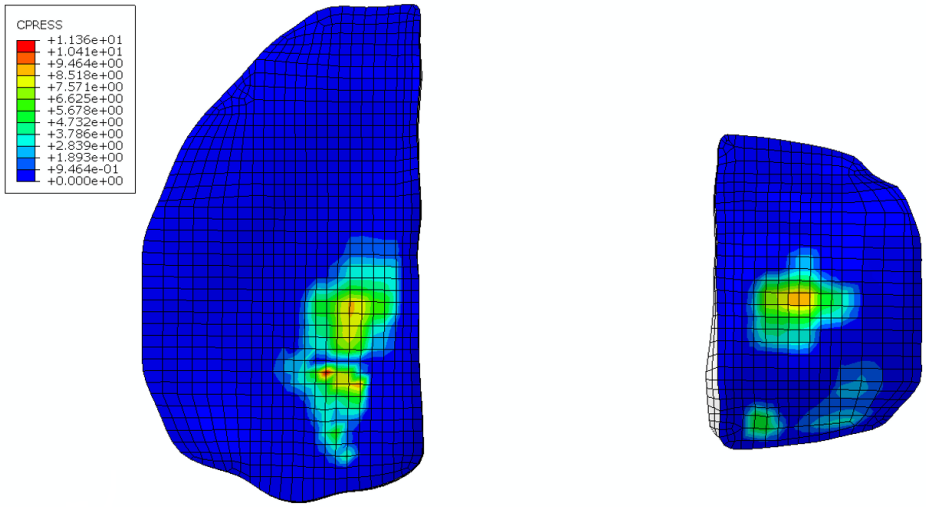

Figure 3.9. Contour plot reporting CPRESS for medial (left) and lateral (right) tibia cartilage pressure for cycling results obtained for participant 2016Nov14 (amputee)

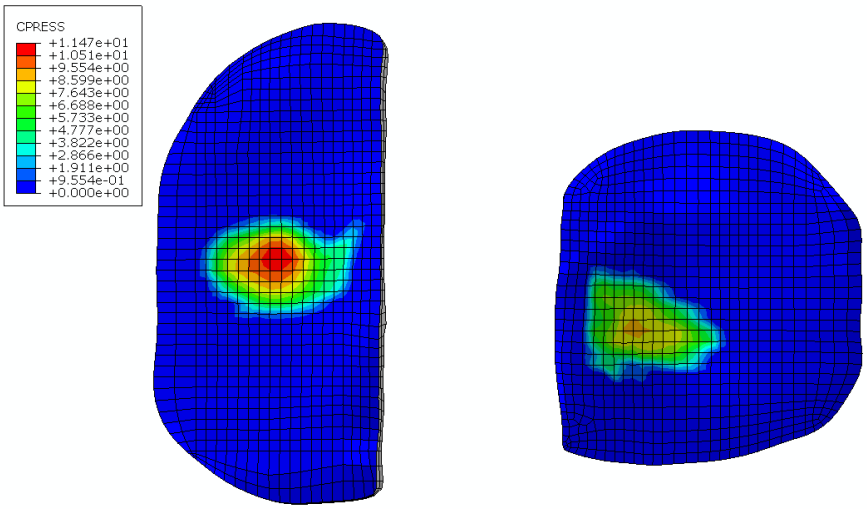

Figure 3.10. Contour plot reporting CPRESS for medial (left) and lateral (right) tibia cartilage pressure for elliptical results obtained for participant 2016Aug12 (control)

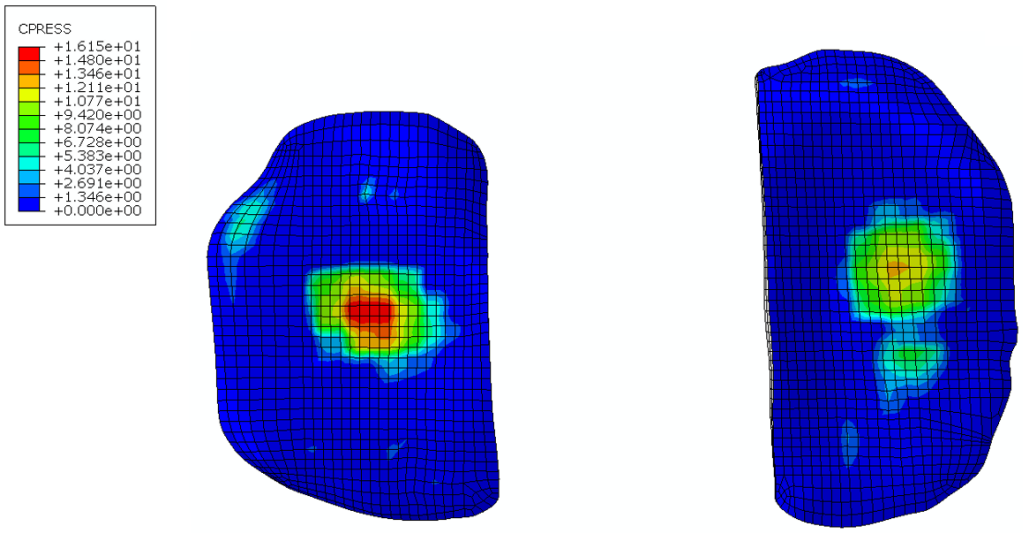

Figure 3.11. Contour plot reporting CPRESS for lateral (left) and medial (right) tibia cartilage pressure for elliptical results obtained for participant 2016Nov10 (amputee)

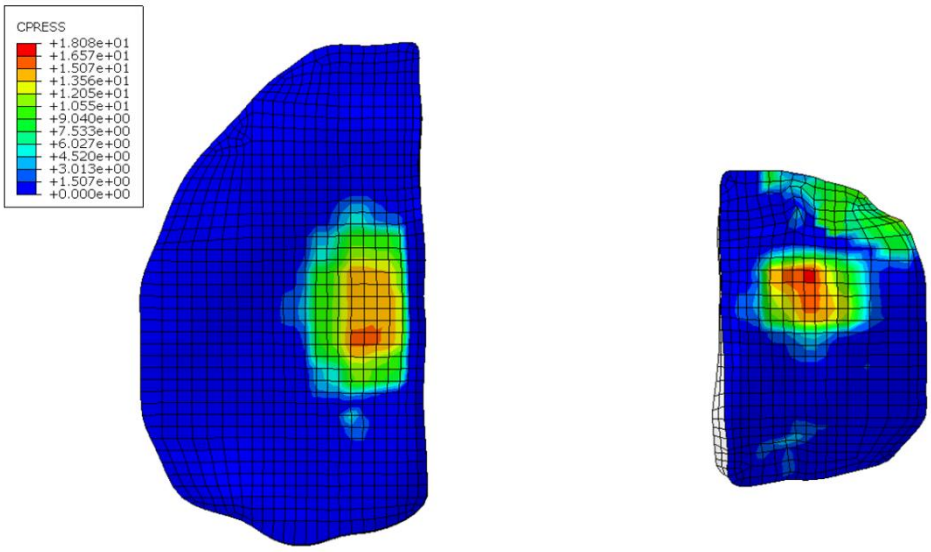

Figure 3.12. Contour plot reporting CPRESS for medial (left) and lateral (right) tibia cartilage pressure for elliptical results obtained for participant 2016Nov14 (amputee)

Table 3.3. Joint contact pressure FE results for gait exercise

Participant	Contact Pressure [MPa]		Contact Pressure normalized by bodyweight [MPa/N]	
	Lateral Tibial	Medial Tibial	Lateral Tibial	Medial Tibial
2016Aug12 (control)	11.66	14.12	0.0147	0.0178
2016Nov10 (amputee)	19.14	18.82	0.0255	0.0251

Table 3.4. Joint contact pressure FE results for cycling exercise

Participant	Contact Pressure [MPa]		Contact Pressure normalized by bodyweight [MPa/N]	
	Lateral Tibial	Medial Tibial	Lateral Tibial	Medial Tibial
2016Aug12 (control)	7.44	8.614	0.0094	0.0109
2016Nov10 (amputee)	11.03	14.63	0.0147	0.0195
2016Nov14 (amputee)	9.23	10.17	0.0110	0.0121

Table 3.5. Joint contact pressure FE results for elliptical exercise

Participant	Contact Pressure [MPa]		Contact Pressure normalized by bodyweight [MPa/N]	
	Lateral Tibial	Medial Tibial	Lateral Tibial	Medial Tibial
2016Aug12 (control)	8.85	10.99	0.0112	0.0114
2016Nov10 (amputee)	15.47	11.21	0.0207	0.0149
2016Nov14 (amputee)	16.76	13.93	0.0199	0.0166

The results displayed in Tables 3.3, 3.4, and 3.5 provide significant information regarding the influence of different exercises on the medial and lateral tibia cartilage pressures of each participant. Furthermore, the application of normalized contact pressure enables a comparison of contact pressures among participants. Consistent with our expectations, the normalized contact pressure magnitudes in the articular cartilage of the amputee simulations were higher than those observed in the control model in both the medial and lateral tibial cartilage compartments. Except for one amputee, the medial tibial cartilage is more involved in gait and cycling while the lateral tibial cartilage is more involved in the elliptical exercise. Importantly, the non-normalized contact pressure values demonstrate consistent trends observed in the

normalized values, both in the comparison between the control and amputee groups, as well as across different exercises.

The simulations show that cycling typically resulted in a smaller contact pressure area, while the gait and elliptical models demonstrated a larger contact pressure area (Tables 3.6, 3.7, and 3.8).

Table 3.6. Total surface area [mm^2] (CAREA) of tibial cartilage compartments in contact with femoral cartilage in Gait

Participant	Gait (mm^2)	
	Lateral Tibial	Medial Tibial
2016Aug12 (control)	175.4	173.8
2016Nov10 (amputee)	227.6	221.5
2016Nov14 (amputee)	86.8	94.75

Table 3.7. Total surface area [mm^2] (CAREA) of tibial cartilage compartments in contact with femoral cartilage in Cycling

Participant	Cycling (mm^2)	
	Lateral Tibial	Medial Tibial
2016Aug12 (control)	71.2	103.9
2016Nov10 (amputee)	43.7	89.3
2016Nov14 (amputee)	105.4	95.4

Table 3.8. Total surface area [mm^2] (CAREA) of tibial cartilage compartments in contact with femoral cartilage in Elliptical

Participant	Elliptical (mm^2)	
	Lateral Tibial	Medial Tibial
2016Aug12 (control)	141.2	135.4
2016Nov10 (amputee)	98.7	110.2
2016Nov14 (amputee)	153.3	169.8

4. Discussion

The results from this study indicate that both gait and elliptical exercises generated higher contact pressure in both the medial and lateral tibial cartilage compartments when compared to cycling. Also, cycling typically exhibited smaller tibial cartilage contact pressure area compared to gait and elliptical training. Both of these results indicate the significance of non-impact exercises, like cycling, on cartilage pressure and, subsequently, OA risk. In addition, tibial cartilage pressures for the amputee simulations were higher than those recorded for the control participant, indicating an increased risk for OA in the intact limb of transtibial amputees compared to healthy individuals.

This study's findings align with other research on joint movement, indicating that cycling generates noticeably reduced knee joint forces and rotation moments compared to walking [68], [9]. This observation could be explained by the fact that the compressive forces measured by the motion capture techniques during the cycling and elliptical exercises were typically much lower than those during the gait. These reduced forces and moments during cycling contributed to lower contact pressures on the joints, ultimately suggesting a decreased risk of developing osteoarthritis. Based on the results from this study, reduced cartilage pressure would be expected during cycling compared to gait and elliptical exercises for both healthy individuals and for transtibial amputees.

This study had several novel aspects to it. For the very first time in whole knee FE simulations, realistic material properties were assigned to articular cartilage through a UMAT material subroutine, enhancing the capacity to accurately simulate cartilage behavior under predefined loading conditions. Prior research in [30], [39], and [40] relied on linear elastic material properties, which were not effective in predicting stress and strain within cartilage during activities such as gait, cycling, and elliptical exercises. Another notable enhancement in this study involved the adoption of hexahedral elements, as opposed to the tetrahedral elements used in previous studies in [30], [39], and [40]. The use of hexahedral elements not only reduced the computational cost of the simulation but also significantly mitigated the occurrence of random errors resulting from the severe distortion associated with tetrahedral elements.

4.1 Mesh convergence

As anticipated, the use of coarse meshes led to inaccurate capture of local stress concentrations, primarily due to the larger inter-node distances relative to the point of load application or transmission. This may result in inaccuracies in the stress results, especially when certain element nodes disproportionately contribute to the stress result after averaging. Fine meshes, on the other hand, exhibited higher fidelity in identifying local stress concentration patterns in regions close to the load application. As such, a suitable mesh density was chosen for the cartilage structures to ensure accurate cartilage pressure and contact area results in the models.

4.2 Validation Study

The results of validation studies suggest that the geometry and material modeling in this study accurately reflected realistic physiology to a reasonable extent. Experimental data from Seitz et al. [67] served as a benchmark for validating the FEA results. The differences between the FEA results and the experimental mean values were less than 13.8%, indicating a strong validation of the FEA results against the experimental data. Nonetheless, the validation study does not extend to the ligament methodology as the experiment in Seitz et al. [67] was conducted in a way that likely did not include ligaments. As a result, the accuracy of how ligaments were modeled in this study cannot be verified. Nevertheless, given that the ligament methodology is supported by literature, it is reasonable to accept the FE model results with ligaments included.

4.3 Material Parameter Study

Varying the collagen fiber modulus and volume fraction in the model within acceptable experimental ranges resulted in variations in cartilage contact pressures of less than one percent. Acceptable experimental ranges of the ground matrix shear modulus, on the other hand, had a drastic effect on the resulting cartilage pressure determined by FEA. Using the extremes of the experimental shear modulus range, cartilage contact pressures varied by up to 89%. Ultimately, a suitable value was found for the ground matrix shear modulus in the model by validating the results against the experimental study of Seitz et al. [67], but further experimental work and a more elaborate parameter study are needed to identify the most appropriate values for this and other model variables.

4.4 FEA Results

The main aim of this thesis was to replicate the impact of different exercises, such as gait, stationary cycling, and elliptical training, on the cartilage in the tibiofemoral joint. The focus was on comparing the contact pressure exerted on the cartilage between a healthy individual and individuals with transtibial amputations. To achieve this, subject-specific finite element models were created using MRI scans to obtain personalized geometry and motion analysis experiments were utilized to gather subject-specific joint contact loads. To ensure reliable results, a consistent framework capable of generating robust finite element models that could handle significant deformations was developed.

This architecture represents a significant improvement over previous studies, as it successfully generated converged models by implementing a UMAT user subroutine to define cartilage material properties and replacing tetrahedral elements with hexahedral elements for more accurate results. As a result, it exhibited greater robustness compared to previous whole knee models developed in the HMB lab. In this research, three distinct geometries were created, and nine simulations were conducted, with three simulations for each subject-specific tibiofemoral joint geometry corresponding to the three exercises performed in the motion analysis experiments.

There is a limited amount of research focused on FEA models of the articular contact pressure in the tibiofemoral joint [53]. Furthermore, the number of studies examining cartilage pressure for transtibial amputees is even more restricted. Directly comparing the results of subject-specific finite element simulations becomes challenging due to this limitation. The most comparable findings are presented by Lane [40] and Stearns [30]. Tables 4.1 and 4.2 show the contact pressure results of all three studies for gait and cycling.

Table 4.1. Normalized contact pressure results for gait exercise. Average values from Lane [40] and subject-specific values from Stearns [30] and this thesis.

CPRESS Normalized by bodyweight [MPa/N]	Participant	Medial	Lateral
Lane [32]	Control	0.0157	0.00896
	Amputee	0.0163	0.00883
Stearns [30]	2016Aug12 (control)	0.0176	0.0205
	2016Nov10 (amputee)	0.0284	0.0292
	2016Nov14 (amputee)	0.0240	0.0355
This Study	2016Aug12 (control)	0.0178	0.0147
	2016Nov10 (amputee)	0.0251	0.0255
	2016Nov14 (amputee)	0.0185	0.0219

Table 4.2. Normalized contact pressure results for cycling exercise. Average values from Lane [40] and subject-specific values from Stearns [30] and this thesis.

CPRESS Normalized by bodyweight [MPa/N]	Participant	Medial	Lateral
Lane [32]	Control	0.0119	0.00391
	Amputee	0.0123	0.00363
Stearns [30]	2016Aug12 (control)	0.0183	0.00970
	2016Nov10 (amputee)	0.0182	0.0141
	2016Nov14 (amputee)	0.0170	0.0131
This Study	2016Aug12 (control)	0.0109	0.0094
	2016Nov10 (amputee)	0.0195	0.0147
	2016Nov14 (amputee)	0.0121	0.0110

In this study, almost all contact pressure values were lower than those reported by Stearns [30] (up to 40.43% lower) and higher than those reported by Lane [40] (up to 308% higher). Lane's simulation not only reported average results across all participants but also incorporated joint resultant loads (incorporating the sum of the contact loads, muscle forces, and ligament forces) instead of joint contact loads (the load at the joint contact between the tibia and femur), and these findings are consistent with physiological expectations. Typically, joint contact loads are approximately 200-300 times greater in magnitude compared to joint resultant forces [30]. To provide a clearer understanding of the difference in magnitude between the joint resultant forces applied by Lane and the joint contact loads utilized in this study, Lane employed resultant compression loads ranging from 763 N to 1018 N. In contrast, this study expanded the range of compression loads to a much wider spectrum from 729 N to 4117 N.

This study improves upon Stearns' work [30] in two key ways. Firstly, it utilizes hexahedral elements instead of tetrahedral elements, resulting in more accurate simulations. Secondly, the study incorporates a more suitable material model for cartilage, enhancing the realism of the model. These advancements contributed to a more reliable and comprehensive understanding of cartilage behavior.

When simulating contact pressure, tetrahedral elements approximate the contact area using interconnected triangles. However, due to their geometric limitations, they may not accurately capture complex contact behavior, especially when the contact surfaces don’t align with the tetrahedral mesh. Hexahedral elements, on the other hand, provide a better representation of contact pressure as they approximate the contact area using interconnected quadrilateral faces. This allows for more precise analysis of contact behavior, particularly when the contact surfaces align well with the hexahedral mesh.

In terms of assessing the contact area, it would be more reasonable to compare the contact area between the femoral and tibial cartilages within the same participant for different exercises rather than across different participants. This is because the loads involved in the exercises are extracted at different flexion angles for each individual due to the experimental setup and particular conditions of each participant. This would make it difficult to establish a consistent basis for comparison between participants. Therefore, a more meaningful comparison can be made by examining the differences in contact area for a given exercise for the same participant. The contact areas during walking and while using an elliptical

machine were found to be larger than for cycling for both the medial and lateral compartments. For two participants, walking resulted in a larger contact area than doing the elliptical exercise, while for participant 2016Nov14-02, the contact area was slightly larger during the elliptical exercise. The total contact area was found to be similar between the medial and lateral tibial compartments.

In this study, it is important to note that the applied loads represent only a fraction of the total cartilage loading, as ligament forces play a crucial role. The behavior of the collateral ligaments during high flexion angles might account for the absence of a significant difference in medial contact pressure between gait and cycling. It is worth mentioning that inaccurately defining the ligaments could introduce errors to the model and its outcomes. Furthermore, the varus-valgus and internal-external rotation joint contact moments were not taken into account in this model. This decision was made because the methodology used by Fernandez in [43] only considers forces, neglecting these moments. However, by introducing the varus-valgus moment from Lane [40], the contact pressure is shifted towards the medial compartment, resulting in significantly higher medial contact pressure compared to the lateral contact pressure. Nevertheless, during this thesis, minimal disparities were noticed in the contact pressure when evaluating the two tibial compartments within a single simulation.

Furthermore, several studies have indicated that individuals who have undergone amputation face an increased likelihood of developing osteoarthritis (OA), particularly affecting the medial side [5], [6]. Amputees experienced higher cartilage pressure compared to the control group on both the medial and lateral sides. This held true for both absolute pressure values and when normalized. The increased pressure was observed across all exercises. These findings affirm that elevated contact pressure acts as a significant risk factor for OA in amputees.

Contact pressure alone may not be the only factor that requires investigation in order to determine the precise cause of OA. In fact, there may be other underlying physiological changes specific to amputees that contribute to the increased incidence of OA which cannot be accurately predicted by a FEA model. The examination of cadavers has revealed that forces acting on the ACL vary considerably depending on the angle of flexion and the applied load [69]. This finding was similarly observed in the FEA models. The ligament spring elements exert force based on their relative displacement, which can undergo significant

changes as the knee moves. Consequently, a substantial portion of the stress experienced by the joint surfaces is a result of the forces exerted by the ligaments. It is highly probable that ligaments play a significant role in the risk factors for OA in individuals with TT amputation. Employing subject-specific modeling of the ligaments would be beneficial in further distinguishing differences between the amputee population and the control group.

4.5 Model Limitations

Although the model was meticulously constructed to fulfill all requirements for organic simulation, there is still a need for enhancing the model and obtaining more realistic outcomes. The limitations addressed in this study will be accompanied by proposed opportunities for future research.

4.5.1 Abaqus Analysis Solver

The implementation of a UMAT material model for cartilage demonstrated no significant distinction when compared to using an incompressible elastic material, as employed by Stearns [30], in terms of the immediate response of the material. This observation was made in these models through the utilization of a Static Abaqus Standard Implicit analysis.

Cartilage, being a time-dependent material, exhibits viscoelastic behavior characterized by both time-dependent (viscous) and time-independent (elastic) responses. The Static Abaqus Standard Simulation, employing the Full Newton solution technique, is suitable when the material's response can be considered as time independent. Although it is possible to simulate time-dependent material behavior to some extent within the framework of a static analysis, by using UMAT, it may be more appropriate to consider using Abaqus/Explicit when the analysis heavily relies on complex time-dependent material behavior.

4.5.2 Material Model

A primary objective of the study was to explore the behavior of articular cartilage through computational simulation, employing a more realistic material model. While this was a significant advancement, a more precise model would involve incorporating the triphasic theory, which accounts for the charged and hydrated nature of soft tissues. This theory encompasses a charged and hydrated soft tissue

as a composition consisting of various components: a porous-permeable charged solid phase comprising the extracellular matrix (ECM), collagen fibers, and PGs; a fluid phase represented by water; and an ionic phase encompassing two monovalent species, Na^+ and Cl^-.

The theory assumes that these phases interact simultaneously at each location and are intrinsically incompressible. The governing equations account for the mass, momentum, and charge density of the solid matrix, the interstitial fluid, as well as the cations and anions. The fluxes of fluid and ions are dependent on fluid pressure and ion concentration, respectively, resulting in a fully coupled and highly nonlinear set of differential equations [70].

4.5.3 Meshing

Utilizing the meshing capabilities within Abaqus ensures the consistent application of meshing parameters and techniques across various parts in the analysis. This approach enhances the repeatability of analysis results while minimizing the chances of errors or inconsistencies throughout the analysis process. While leveraging Abaqus' meshing capabilities can be time-saving during the model discretization process, it necessitates preparing the parts before initiating the meshing procedure. This preparation entails partitioning the parts into smaller sections that can be subsequently filled with hexahedral elements. However, this process relies on the operator's skills, which are often acquired through trial and error, making it potentially time-consuming until the operator becomes accustomed to the technique.

4.5.4 Ligaments Definition

The TF joint possesses an intricate network of ligaments that play a crucial role in maintaining stability during physical movements. These ligaments connect both the bones and the menisci. However, in this particular study, the ligament system has been simplified to four non-linear axial springs, drawing from previous research. Ideally, it would be more accurate to model the ligaments as nonlinear anisotropic structures that interact with all components of the TF joint.

A significant contribution to the stiffness of ligaments arises from the friction generated as the ligament bundles wrap around each other and elongate when subjected to tension [71]. Additionally, the presence of synovial fluid around the ligament bundles introduces viscous forces during elongation, further influencing the overall stiffness [72].

Furthermore, there is a scarcity of research supporting the approximation of these ligaments as basic springs. The challenge lies in the fact that determining the material properties of ligaments in vitro significantly differs from their behavior in vivo, making it difficult to accurately quantify their characteristics for finite element simulations.

4.5.5 Load and Boundary Conditions

The hypothesis presented suggests that individuals with TT amputations experience increased pressure on the articular cartilage, leading to tissue degradation. The method used in this study involved considering load conditions based on the point of maximum compressive force, which typically exhibits the highest magnitude compared to shear forces in the anterior-posterior and medial-lateral directions. This assumption implies that the largest compressive force corresponds to significant contact pressure. However, it would be an oversimplification to focus solely on a single time point during activities such as walking, cycling, or elliptical training, as cartilage loading varies throughout the entire movement of the joint, not just at specific time points. This model fails to adequately represent the daily activities that contribute to osteoarthritis. To capture the complete loading behavior of cartilage during routine activities, future studies could utilize Abaqus FEA to analyze multiple steps within the entire cycle. Such an approach would provide a more comprehensive understanding of how cartilage is loaded under typical daily conditions.

5. Conclusion

The goal of this study was to investigate the contact pressure on the articular cartilage tissue in two transtibial amputees and a control group while doing common exercises including gait, stationary cycling, and elliptical training. The contact pressure results from finite element simulations showed when participants are subjected to gait loads, both tibial compartments exhibit the highest contact pressure levels. Subsequently, elliptical movements generate lower contact pressure magnitudes, followed by cycling, with decreasing order of pressure magnitude.

In all exercises, the amputee participants consistently demonstrated higher bodyweight normalized contact pressure in both compartments compared to the control participant. However, the variation between the lateral and medial compartments was not significant enough to establish a clear trend regarding which compartment was more affected by a specific exercise.

Moreover, it was anticipated that cycling, due to lower loads, would result in decreased cartilage contact stress. Although cycling did reduce contact stress in the lateral compartment, it failed to do so in the medial compartment, which is known to be more susceptible to osteoarthritis (OA). These findings indicate that the mechanisms involved in load distribution within the knee may be more complex than initially assumed. Further modeling is necessary to precisely understand how the knee absorbs and distributes loads during these exercises.

Furthermore, this thesis aimed to develop a methodology for generating subject-specific FEA models. Although there are certain limitations that require improvement, the most significant limitation of this study pertained to the incorporation of ligaments into the model, which was derived from less than perfect MRIs and segmentation. This thesis was built upon previous studies conducted at Cal Poly SLO by addressing some of the limitations mentioned in those studies. It addressed these shortcomings by implementing a more accurate and simplified technique of smoothing, employing optimized meshing techniques, specifically utilizing hexahedral meshing, and assigning more realistic material properties to cartilage.

In the future, there is potential for further expansion and enhancement of these techniques to offer greater functionality. With ongoing improvements, the procedures outlined in this thesis can be leveraged to conduct comprehensive subject-specific FEA studies to explore new research objectives.

REFERENCES

[1] R. Altman et al., “Development of criteria for the classification and reporting of osteoarthritis: Classification of osteoarthritis of the knee,” *Arthritis Rheum.*, vol. 29, no. 8, pp. 1039–1049, 1986.

[2] X. Zhao et al., “Clinical, Humanistic, and Economic Burden of Osteoarthritis (OA) Among Noninstitutionalized Adults in the United States (US),” *Value Heal.*, vol. 21, p. S4, 2018.

[3] C. for D. C. and P. (CDC), “Osteoarthritis (OA),” Center for Disease Control. [Online]. Available: https://www.cdc.gov/arthritis/basics/osteoarthritis.htm. [Accessed: 07-July-2020].

[4] M. G. Cisternas, L. Murphy, J. J. Sacks, D. H. Solomon, D. J. Pasta, and C. G. Helmick, “Alternative Methods for Defining Osteoarthritis and the Impact on Estimating Prevalence in a US Population-Based Survey,” *Arthritis Care Res.*, vol. 68, no. 5, pp. 574–580, 2016.

[5] D. C. Norvell et al., “The prevalence of knee pain and symptomatic knee osteoarthritis among veteran traumatic amputees and nonamputees,” *Arch. Phys. Med. Rehabil.*, vol. 86, no. 3, pp. 487–493, 2005.

[6] M. H. Ebrahimzadeh and S. Hariri, “Long-term outcomes of unilateral transtibial amputations,” *Mil. Med.*, vol. 174, no. 6, pp. 593–597, 2009.

[7] A. K. Silverman, N. P. Fey, A. Portillo, J. G. Walden, G. Bosker, and R. R. Neptune, “Compensatory mechanisms in below-knee amputee gait in response to increasing steady-state walking speeds,” *Gait Posture*, vol. 28, no. 4, pp. 602–609, 2008.

[8] J. A. Buckwalter, D. D. Anderson, T. D. Brown, Y. Tochigi, and J. A. Martin, “The Roles of Mechanical Stresses in the Pathogenesis of Osteoarthritis-Implications for Treatment of Joint Injuries,” *Cartilage*, vol. 4, no. 4, pp. 1–9, 2013.

[9] E. A. Heyde, G. Orekhov, A. M. Robinson, S. J. Hazelwood, and S. M. Klisch, “Hip and knee forces for transtibial amputees in gait and cycling,” in 42nd Annual Meeting of the American Society of Biomechanics, 2018.

[10] Z. Z. Teng, O. Trabelsi, I. Ochoa, J. He, J.H. Gillard, M. Doblare, "Anisotropic material behaviors of soft tissues in human trachea: An experimental study," *Journal of Biomechanics.*, vol 45, no. 9, pp 1717-1723, 2012.

[11] N. J. B . Driessen, G. W. M. Peters, J. M. R. J. Huyghe, C. V. C. Bouten, F. P. T. Baaijens, "Remodelling of continuously distributed collagen fibres in soft connective tissues," *Journal of Biomechanics.*, vol 36, no. 8, pp 1151-1158, 2003.

[12] D. D. Sun, X. E. Guo, M. Likhitpanichkul, W. M. Lai, V. C. Mow, "The Influence of the Fixed Negative Charges on Mechanical and Electrical Behaviors of Articular Cartilage Under Unconfined Compression," *Journal of Biomechanical Engineering.*, vol 126, no. 1, pp 6-16, 2004.

[13] A. D. Pearle , R. F. Warren, S. A. Rodeo, "Basic science of articular cartilage and osteoarthritis," *Clin Sports Med..*, vol 24, no. 1, pp 1-12, 2005.

[14] A. J. S. Fox, A. Bedi, S. A. Rodeo, "Basic science of articular cartilage and osteoarthritis," *Clin Sports Med..*, vol 1, no. 6, pp 461-468, 2009.

[15] P. Tanska, M. E. Mononen, and R. K. Korhonen, "A multi-scale finite element model for investigation of chondrocyte mechanics in normal and medial meniscectomy human knee joint during walking*," J. Biomech.*, vol. 48, no. 8, pp. 1397–1406, 2015.

[16] T. F. Besier, G. E. Gold, G. S. Beaupré, S. L. Delp, "A modeling framework to estimate patellofemoral joint cartilage stress in vivo," *Med Clin Sports Exerc.*, vol 37, no. 11, pp 1924-1930, 2005.

[17] D. W. Smith, B. S. Gardiner, J. B. Davidson, A. J. Grodzinsky, "Computational model for the analysis of cartilage and cartilage tissue constructs," *Journal of Tissue Engineering and Regenerative Medicine.*, vol 10, no. 4, pp 334-447, 2013.

[18] W. C. Hayes, L. F. Mockros, "Viscoelastic properties of human articular cartilage," *Journal of Applied Physiology.*, vol 31, no. 4, pp 562-568, 1971.

[19] O. Klets, M, E, Mononen, P. Tanska, M. T. Nieminen, R, K, Korhonen, S, Saarakkala, "Comparison of different material models of articular cartilage in 3D computational modeling of the knee: Data from the Osteoarthritis Initiative," *J Biomech.*, vol 49, no. 16, pp 3891-3900, 2016.

[20] P. Tanska, M. E. Mononen, and R. K. Korhonen, “A multi-scale finite element model for investigation of chondrocyte mechanics in normal and medial meniscectomy human knee joint during walking,” *J. Biomech*., vol. 48, no. 8, pp. 1397–1406, 2015.

[21] V. B. Shim, G. G. Handsfield, W. Fernandez, “Combining in silico and in vitro experiments to characterize the role of fascicle twist in the Achilles tendon,” Scientific Reports., vol. 8, no. 1, pp. 195–204, 2018.

[22] W. C. Hayes, L. F. Mockros, “Importance of depth-wise distribution of collagen and proteoglycans in articular cartilage—A 3D finite element study of stresses and strains in human knee joint,” *Journal of Biomechanics.*, vol 46, no. 6, pp 1184-1192, 2013.

[23] Rumery, M. G., et al. “Finite Element Analysis Predictions of Knee Cartilage Contact Pressure in Gait and Dependence on Material Model Choice.” In World Congress of Biomechanics, 2018.

[24] Rumery, M. G., et al. “ Gait and Cycling Finite Element Predictions of Knee Cartilage Pressure for Linear and Porous Elastic Materials.” In Annual Meeting of the Biomedical Engineering Society, 2018.

[25] M. Adouni, A. Shirazi-Adl, and R. Shirazi, “Computational biodynamics of human knee joint in gait: From muscle forces to cartilage stresses,” *J. Biomech*., vol 45, no. 12, pp 2149-2156, 2012.

[26] J. Soulhat, M. D. Buschmann, A. Shirazi-Adl, “A Fibril-Network-Reinforced Biphasic Model of Cartilage in Unconfined Compression,” *Journal of biomechanical Engineering*., vol 121, no. 3, pp 340-347, 1999.

[27] M. Sylvia, “Development of a Human Tibiofemoral Joint Finite Element Model to Investigate the Effects of Obesity and Malalignment on Joint Contact Pressure,” M.S. thesis, California Polytechnic State University San Luis Obispo, 2015.

[28] N. A. Czapla, “Development and Validation of a Tibiofemoral Joint Finite Element Model and Subsequent Gait Analysis of Intact ACL and ACL Deficient Individuals,” M.S. thesis, California Polytechnic State University San Luis Obispo, 2015.

[29] N. H. Yang, H. Nayeb-Hashemi, P. K. Canavan, A. Vaziri, “Effect of frontal plane tibiofemoral angle on the stress and strain at the knee cartilage during the stance phase of gait,” *J Orthop Res.*, vol 28, no. 12, pp 1539-1547, 2010.

[30] J. Stearns, M.S.Thesis., California Polytechnic State University, San Luis Obispo., 2020.

[31] K. M. Moerman, C. A. Holt, S. L. Evans, and C. K. Simms, “Digital image correlation and finite element modelling as a method to determine mechanical properties of human soft tissue in vivo,” J. Biomech., vol. 42, no. 8, pp. 1150–1153, May 2009.

[32] L. Li, S. Patil, N. Steklov, W. Bae, D. DD, R. Sah, and B. J. Freg, “Predicting In Vitro Articular Cartilage Wear in the Patellofemoral Joint using Finite Element Modeling,” in 36th Annual Meeting of the American Society of Biomechanics, 2012.

[33] B. Jones, C. T. Hung, and G. Ateshian, “Biphasic Analysis of Cartilage Stresses in the Patellofemoral Joint,” *J. Knee Surg*., vol. 29, 92–98, 2015.

[34] M. Taffetani, M. Griebel, D. Gastaldi, S. M. Klisch, and P. Vena, “Poroviscoelastic finite element model including continuous fiber distribution for the simulation of nanoindentation tests on articular.

cartilage,” *J. Mech. Behav. Biomed. Mater*., vol. 32, pp. 17–30, 2014.

[35] K. S. Halonen, M. E. Mononen, J. S. Jurvelin, J. Töyräs, and R. K. Korhonen, “Importance of depth-wise distribution of collagen and proteoglycans in articular cartilage—A 3D finite element study of stresses and strains in human knee joint,” *J. Biomech*., vol. 46, no. 6, pp. 1184– 1192, Apr. 2013.

[36] M. E. Mononen, M. T. Mikkola, P. Julkunen, R. Ojala, M. T. Nieminen, J. S. Jurvelin, and R. K. Korhonen, “Effect of superficial collagen patterns and fibrillation of femoral articular cartilage on knee joint mechanics-A 3D finite element analysis,” *J. Biomech*., vol. 45, no. 3, pp. 579– 587, 2012.

[37] J. J. Elias and A. J. Cosgarea, “Computational Modeling: An Alternative Approach for Investigating Patellofemoral Mechanics,” *Sports Med. Arthrosc*., vol. 15, no. 2, pp. 89–94, 2007.

[38] A. A. Ali, S. S. Shalhoub, A. J. Cyr, C. K. Fitzpatrick, L. P. Maletsky, P. J. Rullkoetter, and K. B. Shelburne, “Validation of predicted patellofemoral mechanics in a finite element model of the healthy and cruciate-deficient knee,” *J. Biomech.*, vol. 49, no. 2, pp. 302–309, 2016.

[39] S. D. Wangerin, “Development and Validation of a Human Knee Joint Finite Element Model for Tissue Stress and Strain Predictions During Exercise,” M.S. thesis, California Polytechnic State University San Luis Obispo, 2013.

[40] G. Lane, “Human knee FEA model for transtibial amputee tibial cartilage pressure in gait and cycling,” M.S. thesis, California Polytechnic State University San Luis Obispo, 2018.

[41] M. Stender,. M.S. thesis, California Polytechnic State University San Luis Obispo, 2018.

[42] W. Wilson, J. M. Huyghe, C. C. van Donkelaar, “Depth-dependent Compressive Equilibrium Properties of Articular Cartilage Explained by its Composition,” *Biomechanics and Modeling in Mechanobiology*., vol. 15, pp. 43–53, 2007.

[43]R. Fernandez, S. Biglari, C. O’Hara, S. J. Hazelwood, and S. M. Klisch, “Knee Joint Contact Compressive Force of Transtibial Amputee and Control Participants in Gait, Cycling, and Elliptical. Southwest American College of Sports Medicine Regional Chapter Annual Meeting, 2019.

[44] G. Orekhov, A. M. Robinson, S. J Hazelwood, S. M. Klisch, “Knee joint biomechanics in transtibial amputees in gait, cycling, and elliptical training,” *Plos One*., vol. 14, no. 12, 2019.

[45] K. Dudum, “Placing Markers in Accordance with Enhanced Helen Hayes.” 2015.

[46] S. L. Delp et al., “OpenSim: Open-source software to create and analyze dynamic simulations of movement,” *IEEE Trans. Biomed. Eng*., vol. 54, no. 11, pp. 1940–1950, 2007.

[47] P. A. Yushkevich et al., “User-guided 3D active contour segmentation of anatomical structures: Significantly improved efficiency and reliability,” *Neuroimage,* vol. 31, no. 3, pp. 1116–1128, 2006.

[48] C. Geuzaine and J. F. Remacle, “Gmsh: A 3-D finite element mesh generator with built-in pre- and post-processing facilities,” Int. J. Numer. Methods Eng., vol. 79, pp. 1309–1331, 2009.

[49] H. Si, “TetGen, a Quality Tetrahedral Mesh Generator,” *AMC Trans. Math. Softw*., vol. 41, no. 2, pp. 11, 2015.

[50] H. Si, “TetGen: A quality tetrahedral mesh generator and a 3D Delaunay triangulator,” UR L http//tetgen. berlios., no. 13, pp. vii + 97, 2013.

[51] Smith, M. (2009). ABAQUS/Standard User's Manual, Version 6.9.

[52] M. Adouni, A. Shirazi-Adl, and R. Shirazi, “Computational biodynamics of human knee joint in gait: From muscle forces to cartilage stresses,” *J. Biomech*., vol. 45, no. 12, pp. 2149–2156, 2012.

[53] T. L. Haut Donahue et al., “A Finite Element Model of the Human Knee Joint for the Study of Tibio-Femoral Contact,” *J. Biomech.*, vol. 124, no. 3, pp. 273, 2002.

[54] H. Lipshitz, R. Etheredge, M. J. Glimcher, “In vitro wear of articular cartilage,” *J. Bone Joint Surg Am.* , vol. 57, no. 4, p. 527-534, 1975.

[55] A. Maroudas, P. Bullough, “Permeability of articular cartilage,” *Nature.* , vol. 219, pp. 1260-1261, 1968.

[56] V. C. Mow, M. H. Holmes, W. M. Lai, “Fluid transport and mechanical properties of articular cartilage,” *J. Biomech*., vol. 17, no. 5 pp. 377-394, 1984.

[57] D. R. Eyre, “The collagens of articular cartilage,” *Semin Arthritis Rheum.*, vol. 3, no. 2 pp. 2-11, 1991.

[58] L. Yang, Ph.D. thesis, , University of Twente, Enschede, The Netherlands, 2008.

[59] S. M. Elhamian, M. Alizadeh, M. Shokrieh, “The effect of collagen fibers volume fraction on the mechanical properties of articular cartilage by micromechanics models,” *Perfusion.*, vol. 30, no. 7 pp. 1-9, 2014.

[60] B. A. Rogers, C. L. Murphy, S. R. Cannon, T. W. R. Briggs, “Topographical variation in glycosaminoglycan content in human articular cartilage,” *J Bone Joint Surg Br*., vol. 88, no. 12 pp. 1670-1674, 2006.

[61] A. E. Peters, R. Akhtar, E. J. Comerford, K. T. Bates , “The effect of ageing and osteoarthritis on the mechanical properties of cartilage and bone in the human knee joint,” *Sci Rep.*, vol. 8, no. 1 pp. 5931, 2018.

[62] D. Butler, M. Kay, and D. Stouffer, “Fascicle-Bone Units from human patellar tendon and knee ligaments,” *J. Biomech*., vol. 19, no. 6, pp. 425–432, 1986.

[63] E. Peña, B. Calvo, M. A. Martínez, and M. Doblaré, “A three-dimensional finite element analysis of the combined behavior of ligaments and menisci in the healthy human knee joint,” *J. Biomech.*, vol. 39, no. 9, pp. 1686–1701, 2006.

[64] J. Chahla, Evidence-Based Management of Complex Knee Injuries., Elsevier. Restoring the Anatomy to Achieve Best Outcomes, 2020.

[65] M. Kazemi, L. P. Li, M. D. Buschmann, and P. Savard, “Partial Meniscectomy Changes Fluid Pressurization in Articular Cartilage in Human Knees,” *J. Biomech*., vol. 134, no. 2, (10 pages), 2012.

[66] A. Baliunas, D. Hurwitz, A. Ryals, A. Karrar, J. Case, J. Block, and T. Andriacchi, “Increased knee joint loads during walking are present in subjects with knee osteoarthritis,” *Osteoarthr. Cartil*., vol. 10, no. 7, pp. 573–579, Jul. 2002.

[67] A. M. Seitz, A. Lubomierski, B. Friemert, A. Ignatius, and L. Dürselen, “Effect of partial meniscectomy at the medial posterior horn on tibiofemoral contact mechanics and meniscal hoop strains in human knees,” *J. Orthop. Res*., vol. 30, no. 6, pp. 934–942, 2012.

[68] M. V. Pottinger, K. Mavrommati, S. J. Hazelwood, and S. M. Klisch, “EMG-driven inverse dynamic analysis of knee contact forces during gait and cycling using OpenSim,” in Summer Biomechanics, Bioengineering & Biotransport Conference, 2017.

[69] K. L. Markolf, D. M. Burchfield, M. M. Shapiro, M. F. Shepard, G. A. M. Finerman, and J. L. Slauterbeck, “Combined knee loading states that generate high anterior cruciate ligament forces*,” J. Orthop*. Res., vol. 13, no. 6, pp. 930–935, 1995.

[70] M.H. Doweidar, M. Doblaré, Chapter 3 - Finite Element Modeling and Simulation of the Multiphysic Behavior of Articular Cartilage., Elsevier., Numerical Methods and Advanced Simulation in Biomechanics and Biological Processes, Academic Press, pp. 37-53, 2018.

[71] J. Weiss, J. C. Gardiner, “Computational Modeling of Ligament Mechanics,” *Critical Reviews™ in Biomedical Engineering*, vol. 29, no. 3, pp 303-371, 2001.

[72] P. S. MacWilliams, K. R. Friedrichs, “Laboratory evaluation and interpretation of synovial fluid,” Veterinary Clinics of North America: Small Animal Practice, vol. 33, no. 1, pp 153-178, 2005.

APPENDIX A: Model Constituents

Model Constituents

The composition of articular cartilage structure encompasses three distinct elements: proteoglycan (GAG), collagen (COL), and the ground substance matrix (MAT). The subsequent section elucidates the core principles that underlie these constituents.

Proteoglycan Modeling

Stender formulated a Cauchy stress function for proteoglycans by employing the Poisson-Boltzmann cell model, which accounts for osmotic swelling pressure. Through a process of fitting curves to the model's predictions, the resulting Cauchy stress expression can be represented as follows:

$$T^{GAG} = -\alpha_1(\rho^{GAG})^{\alpha_2} I$$

Here, ρ^{GAG} represents the apparent density of GAG in the present configuration, with α_1 and α_2 being material constants. COL is represented as an uninterrupted arrangement of collagen fibers utilizing a volume fraction across all material points. This approach was established by Shirazi et al. [58] and elaborated upon by Stender. An overview of this method is presented below.

$$T^{COL} = \int_V R(\theta, \varphi) H \sigma_N N \otimes N \, dV$$

Here, σ_N denotes the one-dimensional fiber stress, N represents the unit normal in the reference configuration, $\otimes$ signifies the dyadic product, and H is the Heaviside step function, ensuring that COL solely bears tensile load.

$$H = \begin{cases} 0 & E_N < 0 \\ 1 & E_N \geq 1 \end{cases}$$

Here, E_N denotes the Lagrangian strain along the direction of the fiber.

$$E_N = EN.N.$$

Ground Substance Matrix

MAT is designed to encompass all the mechanical properties of the substance that aren't accounted for by the GAG or COL relationships. The selected model to describe MAT is the Neo-Hookean solid. Stender demonstrates that the second Piola-Kirchhoff stress expression for this material is as follows:

$$S^{MAT} = \mu(I - C^{-1})$$

Here, μ represents the shear modulus of MAT. This value is converted into Cauchy stress, resulting in the following expression:

$$T^{MAT} = \frac{1}{J} F[\mu(I - C^{-1})]F.$$

Stress Balance

The concept of stress equilibrium is a prevalent presumption in continuum mixture theory. This proposition asserts that the stress within the substance is equivalent to the cumulative stress of its individual constituents.

$$T^{SM} = T^{GAG} + T^{COL} + T^{MAT}.$$

APPENDIX B: UMAT Fortran Code

An Abaqus UMAT describing the material behavior of cartilage was utilized by this study. This UMAT code is available upon request by contacting Dr. Stephen Klisch at sklisch@calpoly.edu or Dr. Scott Hazelwood at shazelwo@calpoly.edu.